Kamal Elmokhtar Bennur

EMPIRICAL MODELS FOR PREDICTING KINEMATIC VISCOSITY AND DENSITY OF BIODIESEL-PETROLEUM DIESEL BLENDS

NEU
2017

EMPIRICAL MODELS FOR PREDICTING KINEMATIC VISCOSITY AND DENSITY OF BIODIESEL-PETROLEUM DIESEL BLENDS

A THESIS SUBMITTED TO THE GRADUATE SCHOOL OF APPLIED SCIENCES

OF

NEAR EAST UNIVERSITY

By

Kamal Elmokhtar Bennur

In Partial Fulfillment of the Requirements for the Degree of Master of Science in Mechanical Engineering

NICOSIA, 2017

EMPIRICAL MODELS FOR PREDICTING KINEMATIC VISCOSITY AND DENSITY OF BIODIESEL-PETROLEUM DIESEL BLENDS

A THESIS SUBMITTED TO THE GRADUATE SCHOOL OF APPLIED SCIENCES

OF

NEAR EAST UNIVERSITY

By

Kamal Elmokhtar Bennur

In Partial Fulfillment of the Requirements for the Degree of Master of Science in Mechanical Engineering

NICOSIA, 2017

Kamal Elmokhtar Bennur: EMPIRICAL MODELS FOR PREDICTING KINEAMTIC VISOCSITY AND DENSITY OF BIODIESEL-PETROLEUM DIESEL BLENDS

Approval of Director of Graduate School of Applied Sciences

Prof. Dr. Nadire ÇAVUŞ

We certify this thesis is satisfactory for the award of the degree of master of science in Mechanical Engineering

Examining Committee in Charge:

Prof. Dr. Adil AMİRJANOV	Committee Chairman, Software Engineering Department, NEU
Dr. Youssef KASSEM	Mechanical Engineering Department, NEU
Assist. Prof. Dr. Ing. Hüseyin ÇAMUR	Supervisor, Mechanical Engineering Department, NEU

I hereby declare that, all the information in this document has been obtained and presented in accordance with academic rules and ethical conduct. I also declare that, as required by these rules and conduct, I have fully cited and referenced all material and results that are not original to this work.

Name, Last Name :

Signature :

Date:

ACKNOWLEDGEMENTS

First, my acknowledgements go to my supervisor, Assist. Prof. Dr. Hüseyin ÇAMUR, for his helpful expertise, encouragements, and advice during the research period. His amiable disposition, penetrating critiques and consistent mentoring have made my study and stay in Sheffield memorable, indeed I am very grateful.

To my parents, brothers and sisters, I say thank you for all your supports through prayers and advice of encouragements to hold on, especially when my morale was low. I appreciate you all for your genuine concerns.

Last, but not least, I am incredibly grateful to all of my friends for their constant support and encouragement throughout my entire education.

To my parents….

ABSTRACT

Biodiesel is considered as an alternative source of energy obtained from renewable materials. In the present paper, the investigation of the applicability of adaptive neuro-fuzzy inference system (ANFIS), artificial neural network (ANN), radial basis function neural network (RBFNN) and response surface methodology (RSM) approaches for modeling the biodiesel blends property including kinematic viscosity and density at various temperatures and the volume fractions of biodiesel. An experimental database of kinematic viscosity and density of biodiesel blends (biodiesel blend with diesel fuel) were used for developing of models, where the input variables in the network were the temperature and volume fractions of biodiesel. The model results were compared with experimental ones for determining the accuracy of the models. The developed models produced idealized results and were found to be useful for predicting the kinematic viscosity and density of biodiesel blends with a limited number of available data. Moreover, the results suggest that the ANFIS approach can be used successfully for predicting the kinematic viscosity and density of biodiesel blends at various volume fractions and temperature compared to another models.

Keyword: ANFIS; ANN; Biodiesel; density; kinematic viscosity; RBFNN; RSM

ÖZET

Biyodizel yenilenebilir malzemelerden elde edilen alternatif bir enerji kaynağı olarak düşünülür. Mevcut yazıda, uyarlamalı nöron bulanık çıkarım sisteminin uygulanabilirliğinin araştırılması (ANFIS), Yapay sinir ağı (ANN), Radyal taban fonksiyonu sinir ağı (RBFNN), Ve tepki yüzeyi metodolojisi (RSM), Kinematik viskozite ve yoğunluk dahil olmak üzere biyodizelkarışımlarının modellenmesi için çeşitli sıcaklıklarda ve biyodizelin hacim fraksiyonlarındaki yaklaşımlardır. Kinematik viskozite ve biyodizel karışımlarının yoğunluğu deneysel bir veritabanı (Dizel yakıt biyodizel karışımı) modellerin geliştirilmesi için kullanılmıştır. Biyodizelin sıcaklık ve hacim fraksiyonları ağdaki girdi değişkenleridir. Model sonuçlar modellerin doğruluğunu belirlemekıçın deneysel olanlar ile karşılaştırılmıştır. Geliştirilen modeller, sinirli sayıda mevcut veri ile biyodizel karışımları kinematik viskozitesini ve yoğunluğunu tahmin etmek içinideal sonuçlar üretti ve yararlı olduğu bulundu. Dahası, sonuçlar şunu göstermektedir; ANFIS Yaklaşımı, Kinematik viskozite tahmininde farkli hacim fraksiyonlarındabiyodizelkarışımlarının yoğunluğu ve sıcaklığı başka bir modelle karşılaştırıldığında başarılı bir şekilde kullanılabilir.

Anahtar kelime: ANFIS; YSA; Biyodizel; yoğunluk; kinematik viskozite; RBFNN; RSM

TABLE OF CONTENTS

LIST OF TABLES

LIST OF FIGURES

LIST OF SYMBOLS USED

a	Intercept, dimensionless
a_j	Activation of the unit
E	Backward propagation of errors
g	Acceleration gravity, m/s^2
h	Hidden layer
i	Input layer
n	Node number
o	Output layer
p_j	Potential of unit *j*
P_i	Potential of unit *i*
T	Temperature, K or ℃
w_{ij}	Weight of the connection from unit *i* to unit *j*
x	Input data
α	Learning rate
β	Momentum rate
υ	kinematic viscosity, mm^2/s
ρ	density of the liquid, kg/m^3
σ	Sigmoid function

CHAPTER 1
INTRODUCTION

1.1 Background

Increasing environmental consciousness such as the concerns about greenhouse gas, global warming, and emissions and the soaring price of oil associated with the depletion of the world's oil reserves have drawn researchers' interest in alternative renewable/ sustainable energy sources (Demirbas, 2008; Knothe & Steidley, 2007; Ma & A Hanna, 1999).

Vegetable oils, non-edible oils and their derivatives such as biodiesel have received increasing attention due to their promising characteristics. These renewable sources are biodegradable (Ma et al., 1999), carbon neutral (Pinto et al., 2005) and clean-burning fuels (Vicente et al., 2004) with almost-zero sulphur content.

biodiesel is a mixture of mono-alkyl esters of saturated and unsaturated long chain-fatty acids obtained by a transesterification of oils and fats from plant, animal sources (Demirbas, 2008). Both vegetable oils and biodiesel can be directly used in conventional petroleum diesel engine with little modification or fuel modification (Misra & Murthy, 2010). Moreover, when various blends of petroleum diesel and vegetable oils (De Almeida, 2002) or petroleum diesel and biofuels (Cursaru et al., 2011) are used, the engines work without any damage to their parts and without any engine modifications.

One of the most advantage of biodiesel is reduced the level of pollutants (ElSolh, 2011). In addition, biodiesel has become attractive because it is biodegradable (Ma et al., 1999). Biodiesel has higher point, also is non-toxic, and essentially free of sulfur and aromatics than petro-diesel fuel. Furthermore, it improves remarkably the lubricity of diesel in blends. In addtion, it has some disadvantages such as lower heat of combustion and higher cloud point (Benjumea et al., 2008).

Comparing biodiesel with petro-diesel, the density, density, viscosity, cloud point and cetane number of biodiesel is higher than petro-diesel. In general, the main important biodiesel properties are density and viscosity because they have a direct effect on the atomization process during combustion,

Accurate prediction methods are of great practical value in predicting the biodiesel properties and relevant studies can be found in the recent literature. For instance, in the

middle 1960s Gouw and Vlugter (Gouw & Vlugter, 1964) used the Smittenberg relation to estimate the density of saturated methyl esters at 20 ℃and 40 ℃. Allen et al. (Allen et al., 1999) proposed empirical correlations to estimate the viscosity of saturate and unsaturated FAMEs as a quadratic function of their molecular weight. Krisnangkura et al. (2006) fitted empirical equations to predict the temperature-dependent kinematic viscosities of saturated FAMEs as a function of the carbon number in the corresponding fatty acid. Freitas et al. (2011) predicted the kinematic viscosity of biodiesel blends at various temperature using different empirical models. Pratas et al. (2011) predicted the density of 10 biodiesel blends as a function of temperature using a methodology based on the Kay's mixing rule and the group contribution method.

1.2 Research Aims

The aim of this research is to predict the biodiesel properties including the kinematic viscosity and density using

1. ANFIS (Adaptive Neuro Fuzzy Inference System),
2. ANN (Artificial Neural Network),
3. RBF (Radial Basis Function) and
4. RSM (Response Methodology Surface)

Moreover, this study aims to develop mathematical equations to calculate the biodiesel properties including the density and kinematic viscosity and compare the predicted value with predicted values using ANFIS, ANN, RBF and experimental data.

Furthermore, compare RSM model with Geacai et al., 2015, to show the validation of the RSM and to compare the results of the polynomial equation with mathematical equation obtained by Geacai et al., 2015.

1.3 Thesis Outlines

This chapter provides a brief introduction to biodiesel and its importance for human life. In chapter 2, briefly the empirical models and characteristics of them are discussed in details. Chapter 3 is describes the empirical models were used in the work to predict the two important biodiesel properties in term of density and kinematic viscosity. All the results of the predicted data of biodiesel properties are presented in chapter 4 for, followed by a comparison between the experimental data with predicted data of density and kinematic

viscosity, which is the main topic of this work. The thesis ends with conclusions and suggestions for future work in chapter 5.

.

CHAPTER 2
EMPIRICAL MODELS

2.1 Radial Basis Function (RBF)

RBF have been applied to many fields (Nasiri et al., 2013) such as time series forecasting and function approximation which were the first application used RBF.

RBF neural network is a feed forward network which consists of three layers (Figure 2.1)

1. Input layer
2. Hidden layer
3. Output layer

The determination of number of nodes (basis functions) can be composed by the hidden layer. It can be can be selected among several types of functions, but for most applications they are chosen to be Gaussian functions

These types of functions have the property of being local functions, which means that only they function with their centers close to the input patterns will give a response. So, the hidden layer is composed of a variable quantity of nodes, distributed over all the input space. Each node is a Gaussian function, characterized by a centre c and a width r that produces a non-linear output. Let's assume that the inputs of the network are given in a vector of d components, $x = \{x_1, \ldots, x_d\}$,The activation function, $g_j(x)$, is of the form:

$$g_j(x) = \exp\left(-\frac{(x - c_j)^2}{\sigma_j^2}\right); \quad j = 1, 2, \ldots, m \tag{2.1}$$

where c_j is the centre of the activation function and r_j its width.

RBF network design and training is divided into two part (Liu et al., 2011; Taylor, 1996)

1. Number of hidden layer and their structure
2. weights of the output layer

There are several methods for constructing and training a RBF network (Billings & Zheng, 1995; Sarimveis et al., 2002), and optimizing the design parameters, but the most common case is that the number of basis functions has to be given by complex specifications or by means of a trial and error process.

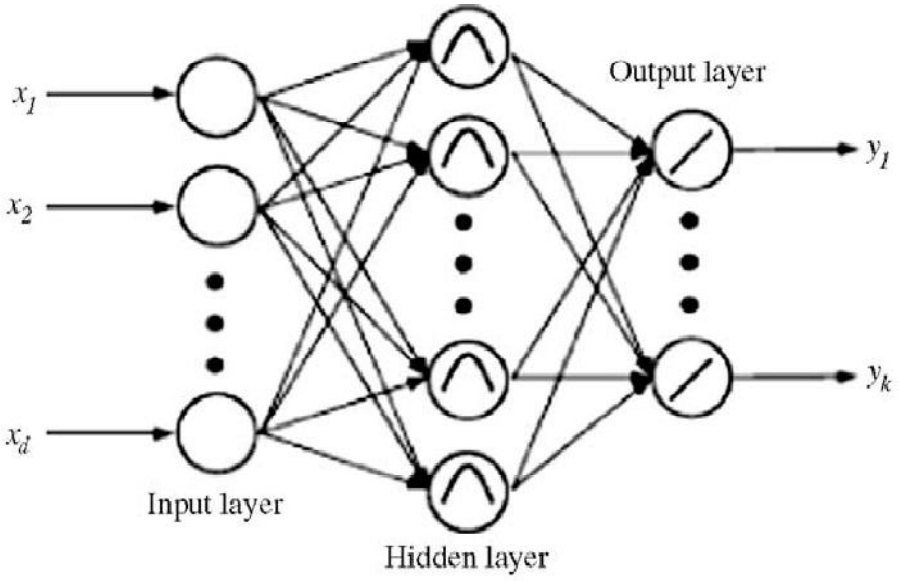

Figure 2.1: RBF network structure (x_d = input to model: y_k = output)

The design of this network is viewed as a curve fitting approximation problem in a high dimensional space. According to this view point, learning is equivalent to finding a surface in a multidimensional space that provides the best fit to the training data. In its most basic form it involves 3 layers with entirely different roles. Input layer is made of source nodes that connect the network to its environment. Second is the hidden layer which applies a nonlinear transformation from the input space to the hidden space, which is of high dimensionality. Output layer is linear, supplying the response of the network to the activation patterns applied to the input layer. Figure 2.1 shows the general architecture of the RBF network. An RBF is symmetrical about a given mean or center in a multidimensional space.

Each RBF unit has two parameters, a center x_j, and a width σ_j. This center is used to compare the network input vector to produce a radially symmetrical response. The width controls the smoothness properties of the interpolating function.

Response of the hidden layer are scaled by the connection weights of the output layer and then combined to produce the network output. In the classical approach to RBF network implementation, the basic functions are usually chosen as Gaussian and the number of

hidden units is fixed based on some properties of the input data. The weights connecting the hidden and output units are estimated by linear least squares method (LMS) (Haykin, 1995).

The strategies for designing RBF network depend on how centers of the radial basis functions of the network are specified (Srinivasa et al., 2003; Srinivasa, 2004).

2.2 Artificial Neural Networks

ANNs is a numerical approach which is based on processing units of artificial neurons that connected together to form a direct graph (Haykin, 2009). Graph nodes is represented the biological neurons while the connections between the neurons is represented synapses.

Whereas, in biological neural networks, connections between artificial neurons aren't usually added or removed after the network was created. As an alternative, the weighted which considered as the connection between the neurons are adapted by ANN approach. Input signal propagates through the network in the direction of connections until it reaches output of the network. In supervised learning, learning algorithm adapts the weights in order to minimize the difference between the output of the network and the predicted output.

2.2.1 Artificial Neuron (AN)

The complex behaviour of biological neurons was clarified to create a empirical model of the units. Unit receives its inputs via input connections from other units' outputs, called activations. Then it calculates a weighted sum of the inputs, called potential. Finally, unit's activation is computed from the potential and sent to other units. Weights of connections between units are stored in a matrix w, where w_{ij} denotes weight of the connection from unit i to unit j. Every unit j has a potential p_j, which is calculated as weighted sum of all of its N input units and bias.

$$P_j = \sum_{i=1}^{N+1} w_{ij} a_i \qquad (2.2)$$

Bias term, also known as threshold unit, is usually represented as an extra input unit whose activation always equals one, therefore $a_{N+1} = 1$. Presence of bias term enables shifting the activation function along x-axis by changing the weight of the connection from threshold unit.

Activation of the unit a_j is then computed by transforming its potential p_j by a non-linear activation function act.

$$a_j = act(P_j) \tag{2.3}$$

Commonly used nonlinear activation function ranging from 0 to 1 is sigmoid function thanks to its easily computable derivative which is used by learning algorithms.

$$\sigma(x) = \frac{1}{1 + e^{-x}} \tag{2.4}$$

$$\frac{d\sigma(x)}{dx} = \sigma(x)(-\sigma(x)) \tag{2.5}$$

where $\sigma(x)$ is sigmoid function, and x is the input data

2.2.2 Feedforward Neural Networks

Feedforward neural networks are a subset of ANNs whose nodes form an acyclic graph where information moves only in one direction, from input to output as shown in Figure 2.2. As shown in Figure 2.2, on the left, Multilayer perception (MLP) consisting of the two inputs, four and three hidden layer and two output layers.

Multilayer perception (MLP) is a class of feedforward networks consisting of three or more layers of units. Layer is a group of units receiving connections from the same units. Units inside a layer are not connected to each other.

MLP consists of three types of layers: input layer (i), one or more hidden layers (h) and the output layer (o). Input layer is the first layer of networks and it receives no connections from other units, but instead holds network's input vector as activation of its units. Input layer is fully connected to the first hidden layer. Hidden layer i is then fully connected to hidden layer $i + 1$. The last hidden layer is fully connected to the output layer. Activation of output units is considered to be output of the network.

The output of the network is calculated in a process called forward propagation in three steps:

Network's input is copied to activations of input units

Hidden layers compute their activations in topological order

Output layer computes its activation and copies it to network's output

MLPs are often used to approximate unknown functions from their inputs to outputs. MLP's capability of approximating any continuous function with support in the unit hypercube with only single hidden layer and the sigmoid activation function was first proved by George Cybenko (Cybenko, 1989).

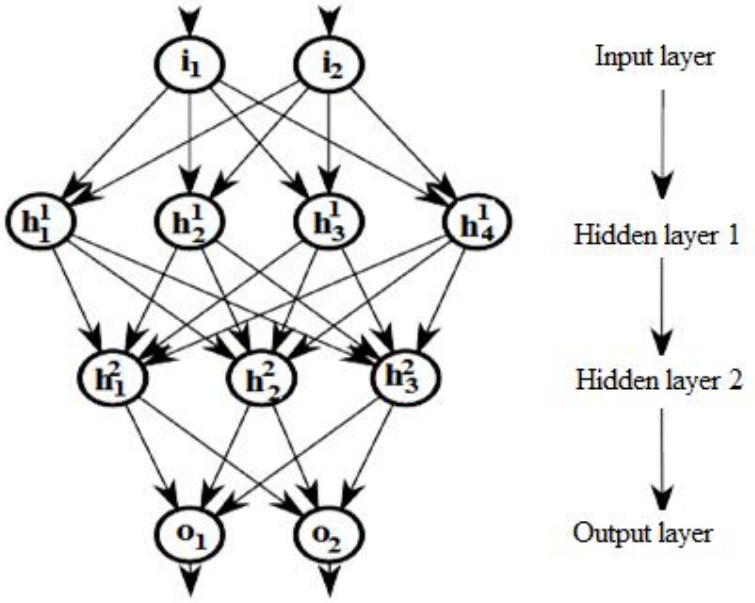

Figure 2.2: Feedforward neural networks

2.2.3 Back-propagation

Back-propagation, or backward propagation of errors, is the most used supervised learning algorithms for adapting connection weights of feedforward ANNs. The weights of the network are tuned so as to minimize square error

$$E = \frac{1}{2}\sum_{i=1}^{N}(target_i - output_i)^2 \qquad (2.4)$$

where target denotes desired the output and output are network's predictions of the output from the corresponding input, both of size N.

Considering error E as a function of network's weights w, backpropogation can be seen as an optimization problem and a standard gradient descent method can be applied. A local minimum is approached by changing weights along the direction of the negative error gradient

$$-\frac{\partial E}{\partial w} \tag{2.6}$$

by weight change Δw_{ij} proportionally to α, which is a constant positive value called the learning rate (α). Fraction of previous weight change called momentum rate (β) can be added to the current weight change, which often speeds up learning process.

$$\text{new } \Delta w_{ij} = \beta \Delta w_{ij} - \alpha \frac{\partial E}{\partial w_{ij}} \tag{2.7}$$

$$new\ w_{ij} = w_{ij} + \Delta w_{ij} \tag{2.8}$$

The central part of the algorithm is finding the error gradient. Let there be an MLP with L layers in topological order, first being input and last being output layer. Layer k has U_k units and holds a weight matrix w_{ij}^k representing weights of connections from unit i in layer k - 1 to unit j in layer k. The input layer has no incoming connections. The computation can be then divided into three steps:

Forward propagation: Input vector is copied to activations a_i^1 of input layer units i. For every hidden or output layer k in topological order, compute for every unit i its potential (weighted input) P_i^k and activation a_i^k

Backward propagation: Compute Δ_i^L i.e. the derivative of error E w.r.t. activation a_i^L of output layer unit i as

$$\Delta_i^L = (target_i - a_i^L) \frac{\partial act(P_i^L)}{\partial P_i^L} \tag{2.9}$$

For hidden layer h in reverse topological order starting from last hidden layer h = L -1 down to first input layer h = 2 and its units i compute error term as

$$\Delta_i = \sum_{j=1}^{U^{+1}} \Delta_i{}^{+1} w_{ij}{}^{+1} \frac{\partial act(P_i)}{\partial P_i} \tag{2.10}$$

Weights update: Change weights in layer k according to

$$\text{new } \Delta w_{ij}^{k} = \beta \Delta w_{ij}^{k} - \alpha \Delta_{i}^{k+1} a_{j}^{k} \quad (2.11)$$

$$\text{new } \Delta w_{ij}^{k} = w_{ij}^{k} + \Delta w_{ij}^{k} \quad (2.12)$$

2.3 Fuzzy Logic Based Algorithms

Fuzzy logic system (FIS) is a technique of rule-based decision making used for expert system and process control. Fuzzy logic is a structure of many-valued logic in which the truth values of variables may be any real number between 0 and 1. Values of one and zero represent the membership of a member to the set with one representing absolute membership and zero representing no membership.

Fuzzy logic allows partial membership, or a degree of membership, which might be any value along the continuum of zero to one. The idea of fuzzy theory is that an is that an element has a degree of membership to a fuzzy set.

As a particular field of application, in system modeling and control. there are many difficulties which are commonly experienced by practicing engineers FIS can be used in different branches such as engineering filed .etc.

In general, FIS consists of three main parts

Fuzzy rules,

Membership function of fuzzy rule, and

Mechanism of Fuzzy interface.

2.3.1 Analysis with Fuzzy Inference System

The following steps are described the procedure for analyzing fuzzy system (Nelles, 2001):

Fuzzification: Fuzzy logic uses input variables as a substitute of numerical variables. The process of converting a numerical variable (real number or crisp variable) into a linguistic variable (fuzzy number) is called fuzzification.

Knowledge Base: This module consists of a data base and a rule base. The data base provides the necessary information for the proper functioning of the fuzzification module, the rule base, and the defuzzification module. This information includes:

Fuzzy sets (membership functions) representing the meaning of the linguistic values of the system state and control input variables.

Physical domains and their nomalized counterparts together with the normalizationl denormalization (scaling) factors.

The basic function of the mle base is to represent the control policy in the form of a set of IF-THEN rules.

Inference Mechanism: This module determined the overall value of the control input based on the individual contributions of each rule in the rule base.

Defuzzification: The reverse of fuzzification is called defuzzification.

2.3.2 Types of Fuzzy System

Fuzzy inference system is based on fuzzy set theory. The two main types of fuzzy system can classified as:

Mamdani fuzzy system: The Mamdani-style fuzzy inference method is carried out in four steps: fuzzification of the input variables, rule evaluation, output of the rule outputs, and finally defuzzification (Castillo & Melin, 2008; Zha & Howlett, 2006).

Singleton Fuzzy system: A singleton is a fuzzy set with a membership function that is unity at a single particular point on the universe of discourse and zero everywhere else. Sugeno-style fuzzy inference is very similar to the Mamdani method. Sugeno changed only a rule consequent (Castillo & Melin, 2008; Zha & Howlett, 2006).

2.3.4 Adaptive Network based Fuzzy Inference System

Adaptive network based fuzzy inference system (ANFIS) is neuron fuzzy technique (Jang, 1993). It has been used as a prime tool in the present work. It is a combination between neural network and fuzzy logic system. The parameters of ANFIS which can be estimated using to models, Sugeno or Tsukamoto, (Tsukamot, 1979) can be presented in architecture of ANFIS.

Again with minor constraints the ANFIS model resembles the Radial basis function network (RBFN) functionally (Jang & Sun, 1993). The methodology of ANFIS includes two techniques

Hybrid system of fuzzy logic

Neural network system

The adaptive network's applications are immediate and immense in various areas. In this proposed work ANFIS was used to predict the thermo-physical properties of biodiesel including kinematic viscosity and density of five biodiesel blends.

2.4. Response Surface Methodology (RSM)

RSM can be described as an empirical modeling system employed for developing, improving, and optimizing complex processes (Manohar & Divakar, 2005). RSM has the advantage of reducing the number of experimental runs, which is sufficient to provide statistically acceptable results (Betiku et al., 2012).

The experimental data obtained from previous studies were analyzed by response surface methodology (RSM) by the response surface regression approach of second-order polynomial equation (Equation (2.13)).

$$Y = P_0 + \sum_{i=1}^{n} P_i x_i + \sum_{i=1}^{n} P_{ii} x_i^2 + \sum_{i}^{n-1} \sum_{i=i+1}^{n} P_{ij} x_i x_j \qquad (2.13)$$

where Y represents the predicted response; βo is the offset term; β_i is the linear coefficient; the second-order coefficient and β_{ij} is the interaction coefficient; x_i and x_j are the independent variables (temperature and volume fraction of biodiesel). The method of least squares was employed to ascertain the values of the model parameters and analysis of variance (ANOVA) was applied to establish their statistical significance at a confidence level of 95%.

CHAPTER 3
METHODOLGY

The main steps that were followed in this work to develop predictive models of density and kinematic viscosity of biodiesel blends as function of temperature and volume fraction of biodiesel are presented

3.1 Experimental database

The databases of this study were formed from results reported in the literature. A total of 900 and 520 experimental points for kinematic viscosity and density, respectively, were obtained from various scientific publications as shown in Table 3.1 to estimate biodiesel properties.

Table 3.1: Biodiesel samples collected from the literature

	Biodiesel Source	Measuring	References
1	**Castor**	Density and kinematic viscosity of biodiesel with different volume fraction of biodiesel at 15℃ and 40℃, respectively.	Amin et al., 2016
2	**Corn and Hazelnut**	Kinematic viscosity of biodiesel samples with different volume fraction of biodiesel in temperature ranges from 10℃ to 40℃.	Gülüm & Bilgin, 2016
3	**Rapeseed**	Kinematic viscosity of biodiesel samples with different volume fraction of biodiesel for each temperature in temperature ranges from 20℃ to 50℃.	Geacai et al., 2015
4	**Soybean, Rapeseed and binary mixture (Soybean and Rapeseed)**	Kinematic viscosity of biodiesel samples with different volume fraction of biodiesel for each temperature in temperature ranges from 20℃ to 120℃ and pressure ranges from 0.1 MPa to 100 MPa.	Freitas et al., 2014

Table 3.1: Continued

	Biodiesel Source	Measuring	References
4	**Sunflowe**	Dynamic viscosity and density of biodiesel samples with different volume fraction of biodiesel for each temperature in temperature ranges from 15℃ to 100℃	Ivaniš et al., 2016
5	**Rapeseed, Sunflower, Soybean, Palm and Corn**	Kinematic viscosity and density of biodiesel samples with different volume fraction of biodiesel for each temperature in temperature ranges from 10℃ to 140℃	Esteban et al., 2012
6	**Peanut and Sunflower**	Kinematic viscosity, density and dynamic viscosity of biodiesel samples with different volume fraction of biodiesel temperature ranges from 15℃ to 100℃	Ramírez-Verduzco et al., 2011
7	**Soybean, Canola, Sunflower, Waste cooking oil and Edible tallow**	Kinematic viscosity, and density of biodiesel samples with different volume fraction of biodiesel in temperature ranges from 20℃ to 80℃	Moradi et al., 2015
8	**Commercially available soybean, natural soybean, modified soybean, yellow grease**	Kinematic viscosity of biodiesel samples with different volume fraction of biodiesel in temperature ranges from 20℃ to 100℃	Yuan et al., 2005
9	**Canola and Soy**	Kinematic viscosity, and density of biodiesel samples in temperature ranges from 20℃ to 300℃	Tate et al, 2006
10	**Soybean and Sunflower**	Dynamic viscosity of biodiesel samples with different volume fraction of biodiesel in temperature ranges from 0℃ to 100℃	Aksoy et al, 2009

Table 3.1: Continued

	Biodiesel Source	Measuring	References
11	**Sunflower, Corn, Soy and Canola**	Kinematic viscosity and density of biodiesel samples with different volume fraction of biodiesel in temperature ranges from 10℃ to 50℃	Machado et al., 2012
12	**Soy A, Soy B, Sunflower, Rapeseed, Palm, and mix of Soy A and Rapeseed**	Dynamic viscosity of biodiesel samples with different volume fraction of biodiesel for each temperature in temperature ranges from 5℃ to 90℃	Freitas et al., 2011
13	**Rapeseed and Used cooking oil**	Density of biodiesel samples with different volume fraction of biodiesel in temperature ranges from 0℃ to 100℃	Barabás, 2013
14	**Corn, Rapeseed and Waste cooking oil**	Density and kinematic viscosity of biodiesel with different volume fraction of biodiesel at 15℃ and 40℃, respectively.	Tesfa et al, 2010
15	**Castor, palm and their blends**	Kinematic viscosity of biodiesel with different volume fraction of biodiesel at 40℃.	Mejía et al., 2013
16	**Sunflower oil, corn oil, pomace oil, soy oil,sesame oil, Jatropha curcas, waste frying oil**	Kinematic viscosity of biodiesel blends with different volume fraction of diesel at 40℃. Additionally, kinematic viscosity and density of pure biodiesel at 40℃ and 15℃, respectively.	Kanaveli et al. 2017

3.2 Empirical Models

In this work, the kinematic viscosity and density of biodiesel blends were modeled using three empirical models as follow:

a) Adaptive Neural Fuzzy Interface System (ANFIS)
b) Artificial Neural Network(ANN)
c) Radial Basis Function Neural Network (RBFNN)
d) Response Surface Methodology (RSM)

The temperature and volume fraction of biodiesel blends were considered as input variables for ANFIS, ANN and RBFNN. As the input variables and output variables for the ANFIS, ANN and RBFNN have different magnitude, a normalization of them is required. A range between 0 and 1 was used as follows

$$\phi_n = \frac{\phi - min(\phi)}{max(\phi) - min(\phi)} \tag{3.1}$$

where ϕ_n is the normalized input or output variable, the minimum (min) and maximum (max) values are shown in Table 3.2.

Table 3.2: Limit values for the input and output variables on the three models

	Limit values	**Unit**
Input value		
Temperature (T)	300-10	℃
Volume fraction of biodiesel	0-1	%
Output value		
Density (ρ)	932.5-508.00	kg/m^3
Kinematic viscosity (ν)	119.48-0.687	mm^2/s

3.3 Appraisal of the developed models

The developed ANFIS, ANN, RBFNN and RSM models were evaluated comprehensively for predictive capability of the response (kinematic viscosity and density) for biodiesel blends. The following statistical indicators were employed: R^2, R, MSE, and RMSE. The results obtained for the three models were compared with one another to determine which one was superior to the other.

$$R = \frac{\sum_i^n \left(a_{p,i} - a_{p,ave}\right) \cdot \left(a_{e,i} - a_{p,ave}\right)}{\sqrt{\left[\sum_i^n \left(a_{p,i} - a_{p,ave}\right)^2\right]\left[\sum_i^n \left(a_{e,i} - a_{p,ave}\right)^2\right]}} \tag{3.2}$$

$$R^2 = 1 - \frac{\sum_{i=1}^n \left(a_{e,i} - a_{p,i}\right)^2}{\sum_{i=1}^n \left(a_{p,i} - a_{e,ave}\right)^2} \tag{3.3}$$

$$MSE = \frac{1}{n}\sum_{i=1}^{n} \left(a_{e,i} - a_{p,i}\right)^2 \tag{3.4}$$

$$RMSE = \sqrt{\frac{1}{n}\sum_{i=1}^{n} \left(a_{e,i} - a_{p,i}\right)^2} \tag{3.5}$$

where n is the number of experimental data, $a_{p,i}$ is the predicted values, $a_{e,i}$ is the experimental values, $a_{e,ave}$ is the average experimental values, $a_{p,ave}$ is the average predicted values and i is the number of input variables.

CHAPTER 4
RESULTS AND DISCUSSIONS

4.1 Adaptive Neuro–Fuzzy Inference System (ANFIS) Model of Density

4.1.1 Method of Applications of ANFIS for Density of Biodiesels

The model was trained with part of the database derived from the experimental results of previous studies. The database was first split into training data and testing data. The training data set was also split into two parts, a training set and a checking set. The use of checking sets in ANFIS learning beside the training set is a recommended technique to guarantee model generalization and to avoid over-fitting the model to the training data set.
In this study, by trial and error (Table 4.1 and Table 4.2), the best number of membership functions for each input was determined as 6, the membership grades takes the Gaussian-shaped membership functions and the output part of each rule uses a constant defuzzifier formula. The numbers of the system parameters of the developed ANFIS model are given in Table 4.3. As can be seen in this table, the number of rules was significantly reduced. Also the optimum method is hybrid. In this research, two methods, hybrid and back propagation tested for generation ANFIS that the results is presented in Tables 4.1 and 4.2. The results show the training error in the hybrid method is lower of back-propagation method. Therefore, the hybrid method has used for simulations.

Table 4.1. The ANFIS information by the hybrid optimum method

Optimum Method	Number of MF	MF type	MF type (output)	Training error	Testing error
Hybrid	2	Gaussmf	Constant	0.0501	0.0411
Hybrid	3	Gaussmf	Constant	0.0484	0.0397
Hybrid	4	Gaussmf	Constant	0.0466	0.0336
Hybrid	5	Gaussmf	Constant	0.047	0.035
Hybrid	6	Gaussmf	Constant	0.0463	0.0327
Hybrid	7	Gaussmf	Constant	0.04626	0.0338
Hybrid	6	Gaussmf	linear	0.0454	0.034

Table 4.2. The ANFIS information by the back-propagation optimum method

Optimum Method	Number of MF	MF type	MF type (output)	Training error	Testing error
back-propagation	2	Gaussmf	Constant	0.051	0.042
back-propagation	3	Gaussmf	Constant	0.0504	0.0416
back-propagation	4	Gaussmf	Constant	0.0504	0.0417
back-propagation	6	Gaussmf	Constant	0.0503	0.0410
back-propagation	6	Gaussmf	linear	0.0497	0.0397

Table 4.3: System parameters of the ANFIS model

ANFIS model parameters	
Number of nodes	101
Number of linear parameters	36
Number of nonlinear parameters	24
Total number of parameters	60
Number of training data pairs	272
Number of checking data pairs	91
Number of fuzzy rules	36

The structure (rules) of the tuned FIS is shown in Figure 4.1, which contains 36 rules with AND logical connector for all rules. In order to develop ANFIS models for designing the density of biodiesel, the available data set from the previous study, which was consisted of two input (temperature and volume fraction of biodiesel with diesel) vectors and their corresponding output vector (density), was used. This data set was randomly assigned as the training set. After training, fuzzy inference calculations of the developed model were performed.

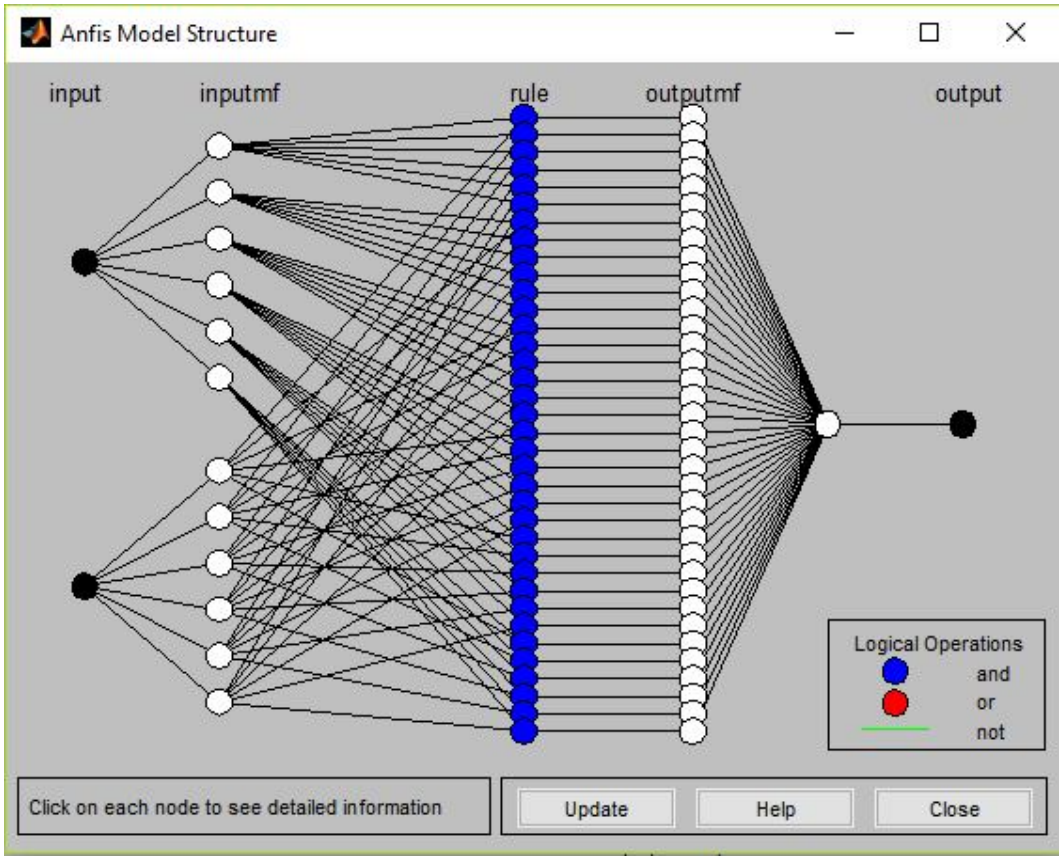

Figure 4.1: Structure of ANFIS models

The ANFIS information and errors which used in this study for predicting the density of biodiesel blends are shown in Table 4.4 that used for all biodiesel blends. The successful training process was accomplished using different training epochs (iterations) for density of biodiesel blends. The ANFIS network was able to achieve training and checking the lowest RMSE (root mean standard error) for density of biodiesel blends. The Figure 4.2 shows training plot achieve with ANFIS for density of biodiesel blends.

Table 4.4: The ANFIS information used in the predicting density of biodiesel by the hybrid optimum method

Biodiesel blend with Diesel	
Epoch	1000
RMSE	
Training error	0.0463
Tasting error	0.0327
Checking error	0.03272

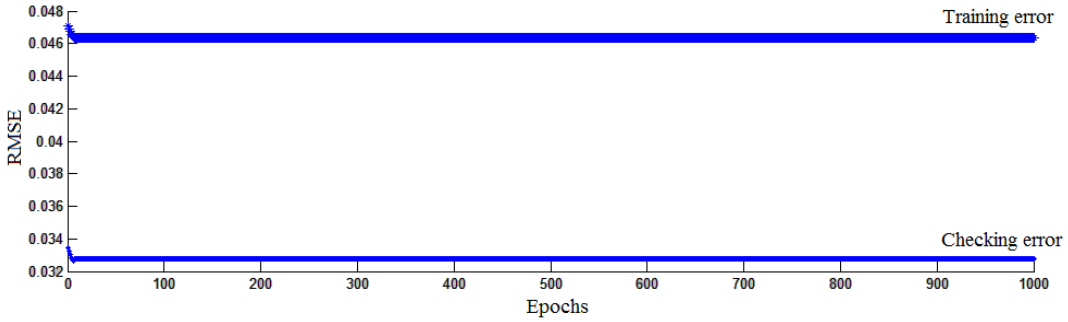

Figure 4.2: Training and checking RMSE achieve with ANFIS for density of biodiesel

Figure 4.3 indicates rule viewers that shows value of the various inputs to the ANFIS models and computed output. The density (output) can be predicted by varying the input parameters, including temperature and volume fraction of biodiesel to the developed ANFIS model.

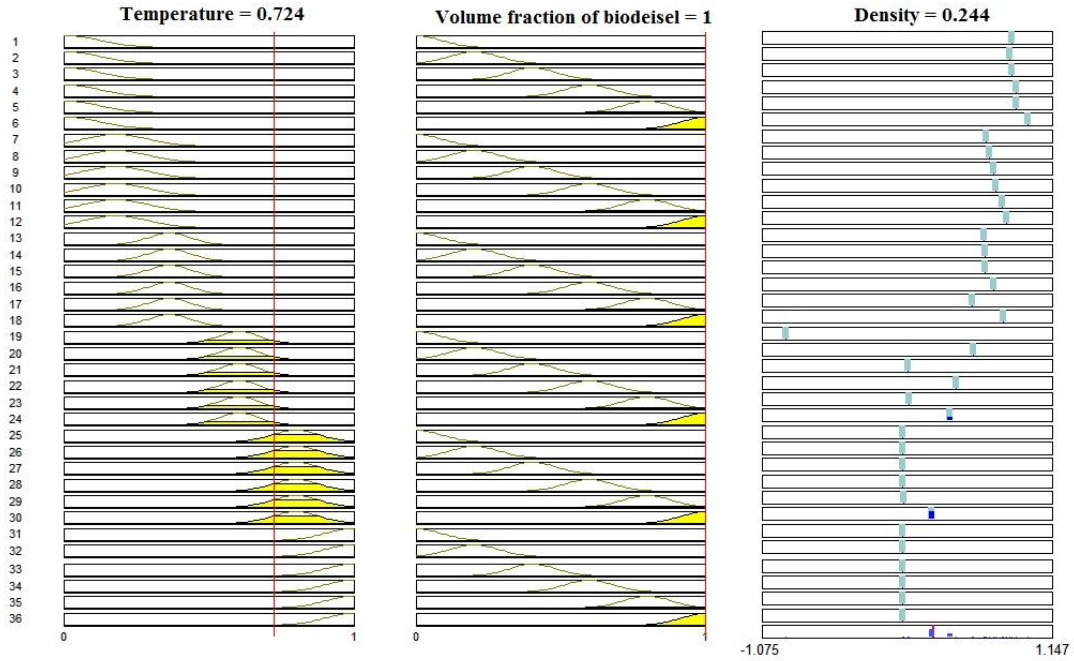

Figure 4.3: Rule viewer of ANFIS model for density of biodiesel blends

The three-dimensional surface plots of kinematic viscosity of biodiesel blend with benzene against temperature and volume fraction of biodiesel is depicted in Figure 4.4 The plot suggest strong interaction between the variables with significant influence on the density of biodiesel blends. From the Figure, increasing in volume fraction of biodiesel leads to increase the density of biodiesel blends, while the lowest temperature leads to decrease the density of biodiesel blends as shown in Figure 4.4.

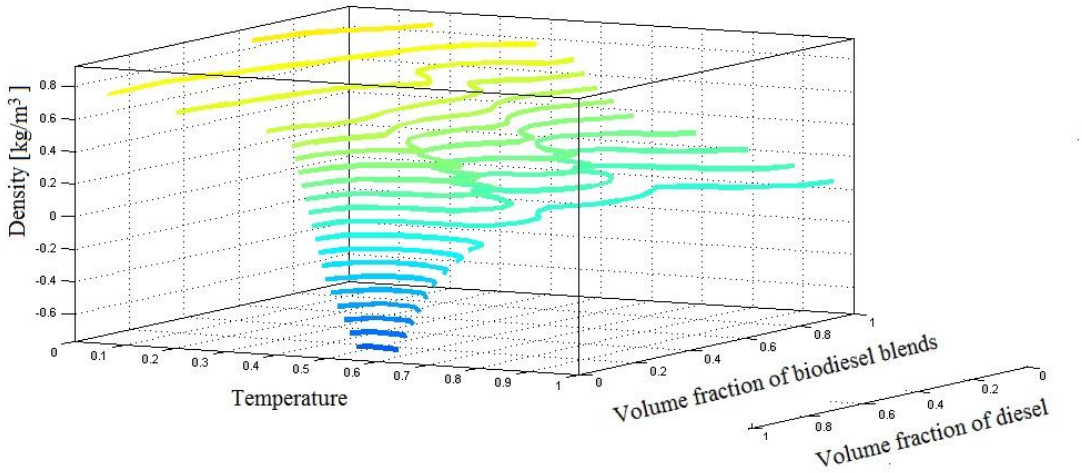

Figure 4.4: Surface viewer of ANFIS model for density of biodiesel blends

4.1.2 Modeling of Density of Biodiesel Blends using ANFIS

Figure 4.5 shows the change of the density with the increase of the percentage of biodiesel. The abscissa represents the fraction of biodiesel, whereas the density values are provided on the ordinate as shown in Figure 4.5. It can be observed from the figure that the density increased as the percentage of biodiesel blend with diesel increased for each temperature considered. Additionally, it can be noticed that increasing temperature leads to decrease the density of biodiesel blends. Moreover, the comparisons of experimental values and ANFIS values of density are shown in 4.5. It can be noticed that the experimental results and the data obtained by ANFIS are very close to each other. Moreover, the maximum absolute relative error between these values is about 4.5%, which indicate an excellent agreement between the experimental and predicting values.

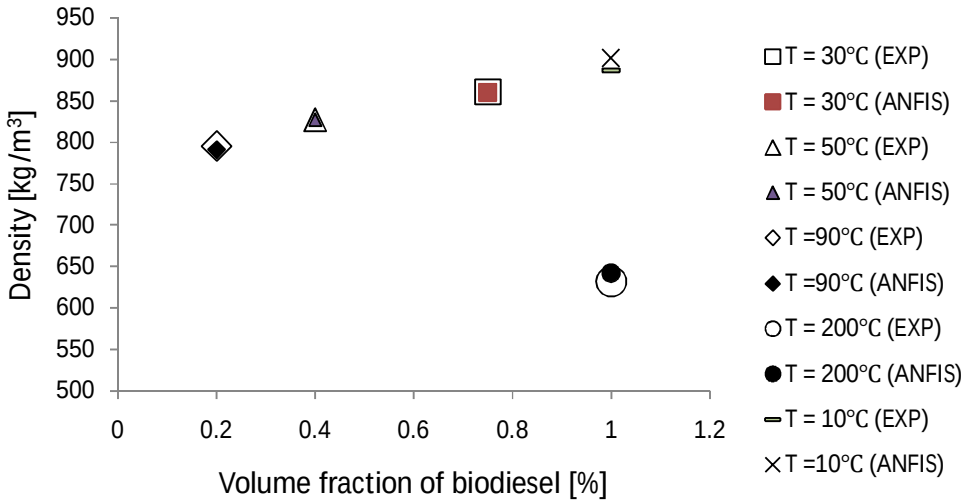

Figure 4.5: Density and volume fraction of biodiesel relationship obtained by ANFIS

Table 4.5: Comparative study between experimental and ANFIS results of biodiesel density

Temperature [□]	Biodiesel fraction	Diesel fraction	Density [kg/m^3]		Absolute error [%]
			EXP	ANFIS	
10	0.5	0.5	829.50	835.29	0.70
	1	0	865.80	859.49	0.73
15	0.5	0.5	884.00	856.52	3.11
	0.2	0.8	860.25	842.08	2.11
	1	0	817.57	818.31	0.09
	0.1	0.9	879.65	898.12	2.10
20	0.01	0.99	834.90	841.23	0.76
	0.25	0.75	832.25	839.96	0.93
	1	0	852.00	865.01	1.53
	0.6	0.4	783.10	782.65	0.06
	0	1	857.94	843.36	1.70
25	0.2	0.8	833.50	835.29	0.21
30	1	0	877.68	887.50	1.12
	0.25	0.75	825.13	859.91	4.21
	0.01	0.99	827.80	832.32	0.55
	0.5	0.5	826.15	828.07	0.23
	0.75	0.25	834.40	841.23	0.82
35	0.2	0.8	857.00	856.52	0.06
40	1	0	874.96	879.86	0.56
	0.5	0.5	837.41	839.11	0.20
	0.1	0.9	825.60	822.98	0.32
50	0.4	0.6	827.00	826.80	0.02
	0.2	0.8	816.50	816.61	0.01
	1	0	631.52	641.72	1.62
	0.8	0.2	879.80	851.85	3.18
	0.25	0.75	785.63	790.29	0.59
55	0.2	0.8	860.65	859.91	0.09
60	0.01	0.99	806.80	804.73	0.26
	0	1	806.20	804.73	0.18
	0.2	0.8	810.00	809.82	0.02
	1	0	848.90	828.07	2.45
	0.6	0.4	832.50	808.97	2.83
65	0.2	0.8	805.15	806.85	0.21
70	0.6	0.4	825.00	824.25	0.09
	0.4	0.6	813.50	813.64	0.02
	0.8	0.2	859.50	839.54	2.32
	1	0	812.14	813.22	0.13

Table 4.5: Continued

Temperature [□]	Biodiesel fraction	Diesel fraction	Density [kg/m^3] EXP	Density [kg/m^3] ANFIS	Absolute error [%]
80	0.8	0.2	826.50	821.28	0.63
	0.2	0.8	796.50	851.85	6.95
	0.15	0.85	871.77	867.98	0.44
	1	0	841.29	846.75	0.65
85	0.1	0.9	831.50	830.62	0.11
90	0.2	0.8	795.10	791.14	0.50
	0	1	785.00	784.35	0.08
	0.6	0.4	815.70	811.52	0.51
	1	0	882.42	894.72	1.39
100	1	0	836.30	845.05	1.05
	0.1	0.9	799.60	795.81	0.47
120	1	0	850.08	859.06	1.06
130	1	0	815.00	835.72	2.54
140	1	0	845.05	853.54	1.01
180	1	0	656.85	653.61	0.49
200	1	0	886.43	901.09	1.65
220	1	0	606.93	611.58	0.77
280	1	0	545.25	531.78	2.47

Furthermore, Figure 4.6 shows the comparisons of ANFIS with experimental results for density of biodiesel blends, which also show good agreement between ANFIS predicted data and experimental data. The R-squared values are also close to unity highlighting proper fitting of the predicted values of density with experimental data.

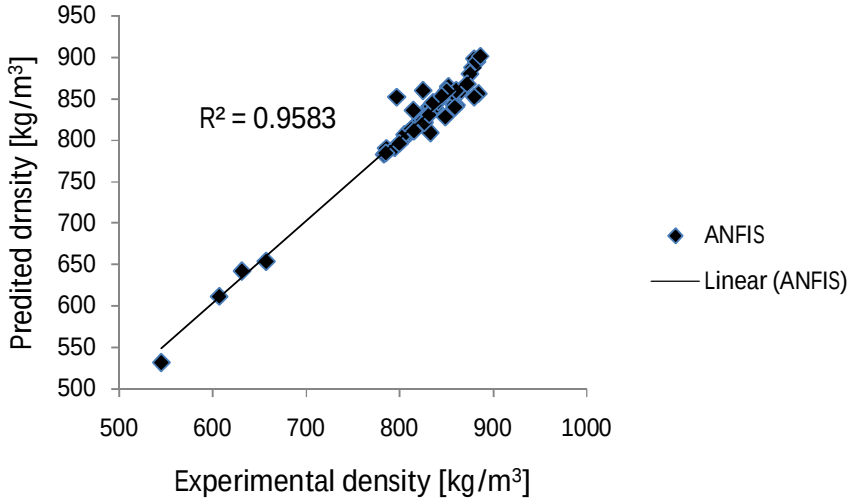

Figure 4.6: Fitting of the predicted ANFIS and experimental values for density of biodiesel blends

4.2 Artificial Neural Network (ANN) Model of Density

4.2.1 Method of Applications of ANN for Density of Biodiesels

The development and the training of the network model in this study were carried out using the MATLAB Neural Network Toolbox. In this study, the experimental data of 454 biodiesel samples were randomly split into three data set, 60% in the training set (272 samples), 20% in the validation set (91 samples) and 20% in the test set (91 samples). The inputs and targets are normalized into the range [-1, 1] to make the training procedure more efficient (Kalogirou, 2001). Training of the network was performed by using the Levenberg–Marquardt, back-propagation algorithms. There is no general rule for the determination of the optimum number of hidden layers and usually it is determined through trial and error method (Moradi et al., 2013). Therefore, the number of neurons in the hidden layer was determined by trial and error test, where a mean squared error greater than 1×10^{-3} and a correlation coefficient higher than 0.9 was obtained. In addition, with the trial and error method, training results showed that the ANN with three hidden layers has the best performance. Consequently, the developed ANN model for predicting density biodiesel blends is shown in Figure 4.7 and the training parameters can be found in Table 5.15. The developed network architecture has a 2-3-1 configuration with two neurons in

the input layer indicating temperature and volume fraction of biodiesel. Three hidden layers with varying neurons and ten neurons in the output layer representing density are used.

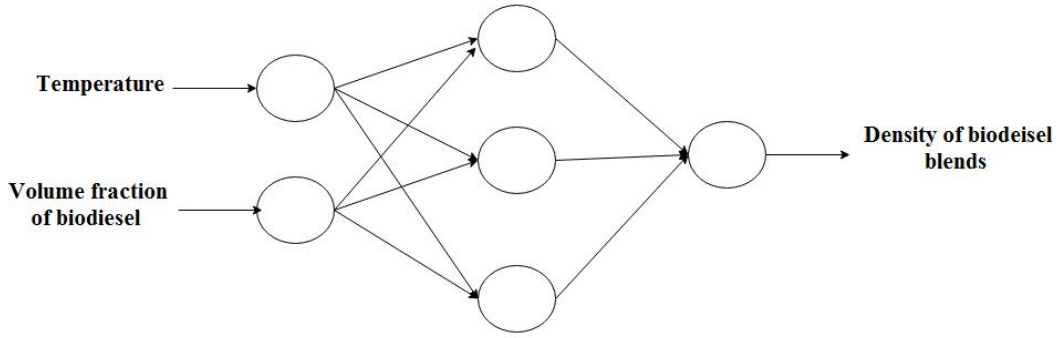

Figure 4.7: Neural network architecture for two inputs and one output

Table 4.6: Neural network configuration for the training

Parameter	Specification
Training Function	Levenberg–Marquardt
Performance function	Mean square error (MSE)
Activation function	Log-Sigmoid
Number of layers	3
Number of neurons	10
Normalized range	-1 to 1

Figure 4.8 illustrates a linear relation for the training, validation, testing and performance of the network with high correlation coefficients (R) of density. The straight lines in Figure 4.8 are the linear relationships obtained between the output (predicted) and the target (experimental) data of density used in this study. The mean squared error (MSE) for density network is 1.16×10^{-3}. The high coefficients of correlation (R) obtained during the training, validation and testing of the density network display very good relationship between the output and the experimental values of density.

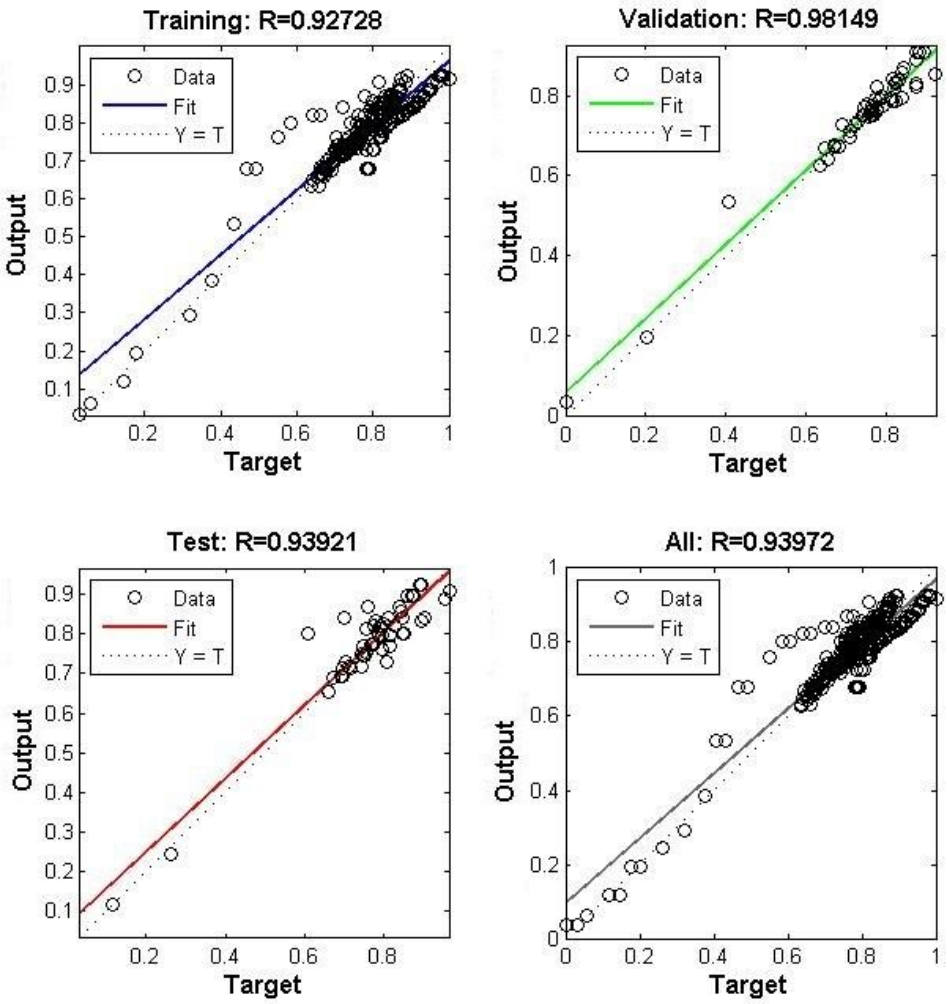

Figure 4.8: Regression plots for density of biodiesel blends network

4.2.2 Modeling of Density of Biodiesel Blends using ANN

The test values obtained from the ANN model results were compared with experimental values as shown in Figures 4.9. As a result, the test values obtained from ANN model were quite compatible with experimental values.

Additionally, the comparisons of experimental values and ANN values of density are given in Table 4.7. It is observed that the experimental results and the data obtained by ANN are very close to each other. Moreover, the maximum absolute relative error is approximately

5% which designate an excellent agreement between the experimental and predicting values.

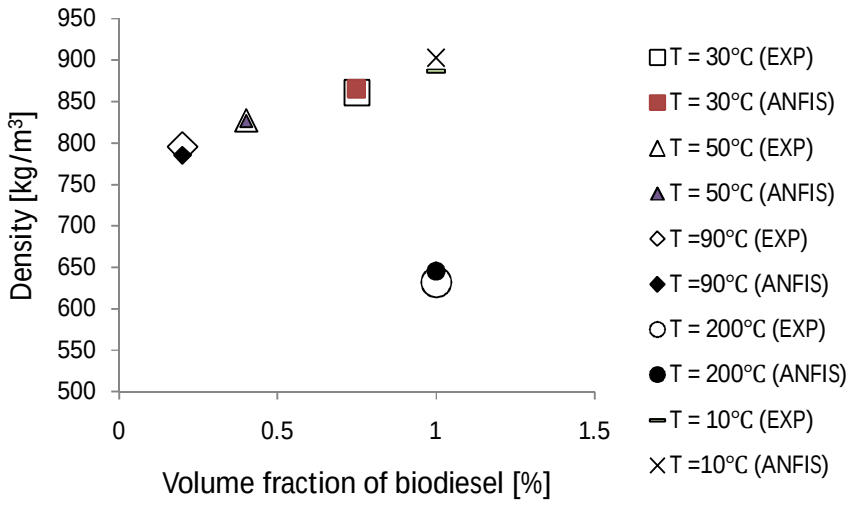

Figure 4.9: Density and volume fraction of biodiesel relationship obtained by ANN

Table 4.7: Comparative study between experimental and ANN results of biodiesel density

Temperature [□]	Biodiesel fraction	Diesel fraction	Density [kg/m^3]		Absolute error [%]
			EXP	ANN	
10	0.5	0.5	829.50	852.68	2.79
	1	0	865.80	868.36	0.30
15	0.5	0.5	884.00	866.06	2.03
	0.2	0.8	860.25	840.46	2.30
	1	0	817.57	825.32	0.95
	0.1	0.9	879.65	846.38	3.78
20	0.01	0.99	834.90	831.64	0.39
	0.25	0.75	832.25	833.86	0.19
	1	0	852.00	855.26	0.38
	0.6	0.4	783.10	782.15	0.12
	0	1	857.94	829.82	3.28
25	0.2	0.8	833.50	835.80	0.28
30	1	0	877.68	886.77	1.04
	0.25	0.75	825.13	829.85	0.57
	0.01	0.99	827.80	824.31	0.42
	0.5	0.5	826.15	848.73	2.73
	0.75	0.25	834.40	864.78	3.64
35	0.2	0.8	857.00	830.47	3.10
40	1	0	874.96	877.99	0.35
	0.5	0.5	837.41	840.66	0.39
	0.1	0.9	825.60	827.52	0.23
50	0.4	0.6	827.00	826.27	0.09
	0.2	0.8	816.50	820.51	0.49
	1	0	631.52	633.00	0.23
	0.8	0.2	879.80	851.10	3.26
	0.25	0.75	785.63	784.39	0.16
55	0.2	0.8	860.65	816.61	5.12
60	0.01	0.99	806.80	805.84	0.12
	0	1	806.20	804.68	0.19
	0.2	0.8	810.00	812.46	0.30
	1	0	848.90	863.59	1.73
	0.6	0.4	832.50	827.09	0.65
65	0.2	0.8	805.15	808.09	0.37
70	0.6	0.4	825.00	821.47	0.43
	0.4	0.6	813.50	803.46	1.23
	0.8	0.2	859.50	827.45	3.73
	1	0	812.14	858.51	5.71

Table 4.7: Continued

Temperature [□]	Biodiesel fraction	Diesel fraction	Density [kg/m^3]		Absolute error [%]
			EXP	ANN	
80	0.8	0.2	826.50	810.16	1.98
	0.2	0.8	796.50	794.35	0.27
	0.15	0.85	871.77	872.33	0.06
	1	0	841.29	854.30	1.55
85	0.1	0.9	831.50	794.83	4.41
90	0.2	0.8	795.10	785.39	1.22
	0	1	785.00	784.30	0.09
	0.6	0.4	815.70	819.78	0.50
	1	0	882.42	850.31	3.64
100	1	0	836.30	845.76	1.13
	0.1	0.9	799.60	785.87	1.72
120	1	0	850.08	831.36	2.20
130	1	0	815.00	819.19	0.51
140	1	0	845.05	801.98	5.10
180	1	0	656.85	690.28	5.09
200	1	0	886.43	885.30	0.13
220	1	0	606.93	616.10	1.51
280	1	0	545.25	534.51	1.97

To evaluate the performances of the ANN modeling further, Figure 4.10 shows the results of fitting the predicted and experimental values for density of biodiesel, using linear regression equations. These clearly show the fit values, and variance of the results predicted by the ANN models has been expressed in terms of R-squared (R^2) values, which are quite encouraging. R-squared value is a measure of goodness-of-fit, which means how close the data points are to the fitted regression line. These values are close to unity, as shown in Figure 4.10, highlighting proper fitting of the predicted values by the adopted methodology.

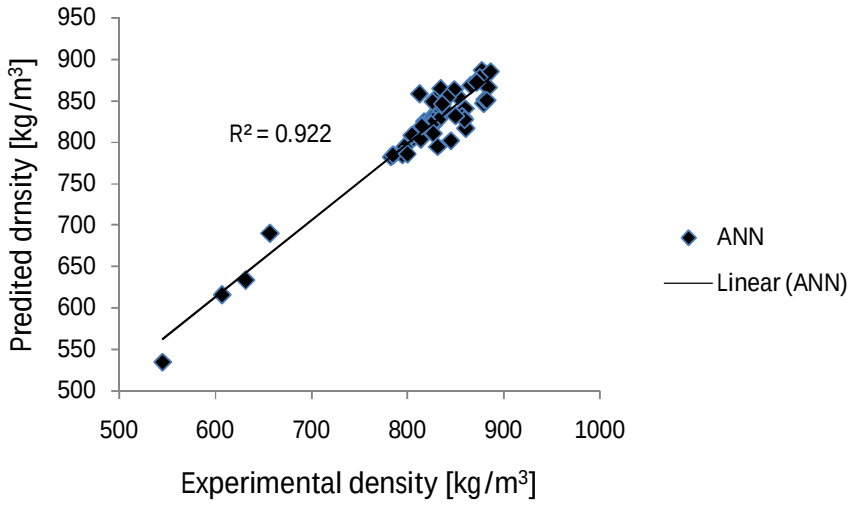

Figure 4.10: Fitting of the predicted ANN and experimental values for density of biodiesel blends

4.3 Radial Basis Function Neural Network (RBFNN) Model

4.3.1 Method of Applications of RBFNN for Density of Biodiesels

The construction of a Radial Basis Function network in its most basic form involves three entirely different layers. The input layer is made up of source nodes (sensory units). The second layer is a hidden layer of high enough dimension, which serves a different purpose from that in a multi-layer perceptron. The output layer supplies the response of the network to the activation patterns applied to the input layer. The RBF network is a single hidden-layer feed forward neural network. The developed network architecture with two input layer indicating temperature and volume fraction of biodiesel and one output (density of biodiesel blends) is shown in Figure 4.11.

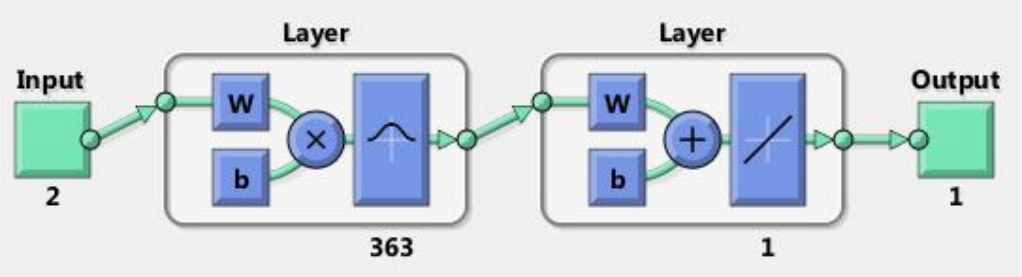

Figure 4.11: RBFNN architecture for two inputs and one output

The network of RBFNN model was trained using two approaches as follow

1. Radial basis (few neurons)
2. Radial basis (exact fit)

MATLAB 13a toolbox has been used for developing the RBF network implementation. Training of the first approach was stopped when either of the performance goals was reached. Training of the network has been done with different number of RBF units. Training of the network has been done with different number of RBF units. For various values of spread (unit) the network error was analyzed it was observed that for a spread of 1, the error was minimum. The network was trained with optimum number of centers determined from the random selection method and a spread of 1. Results for the various performances of the two approaches are presented in Figure 4.12 and tabulated in Table 4.8. It can be seen that it can be observed that *R-squared* and mean squared error (MSE) of RBFNN testing and training results, respectively using two approaches are equal and the model of spread of 1 has a maximum R^2 comparing to another models as shown in Figure 4.12 and Table 4.8.

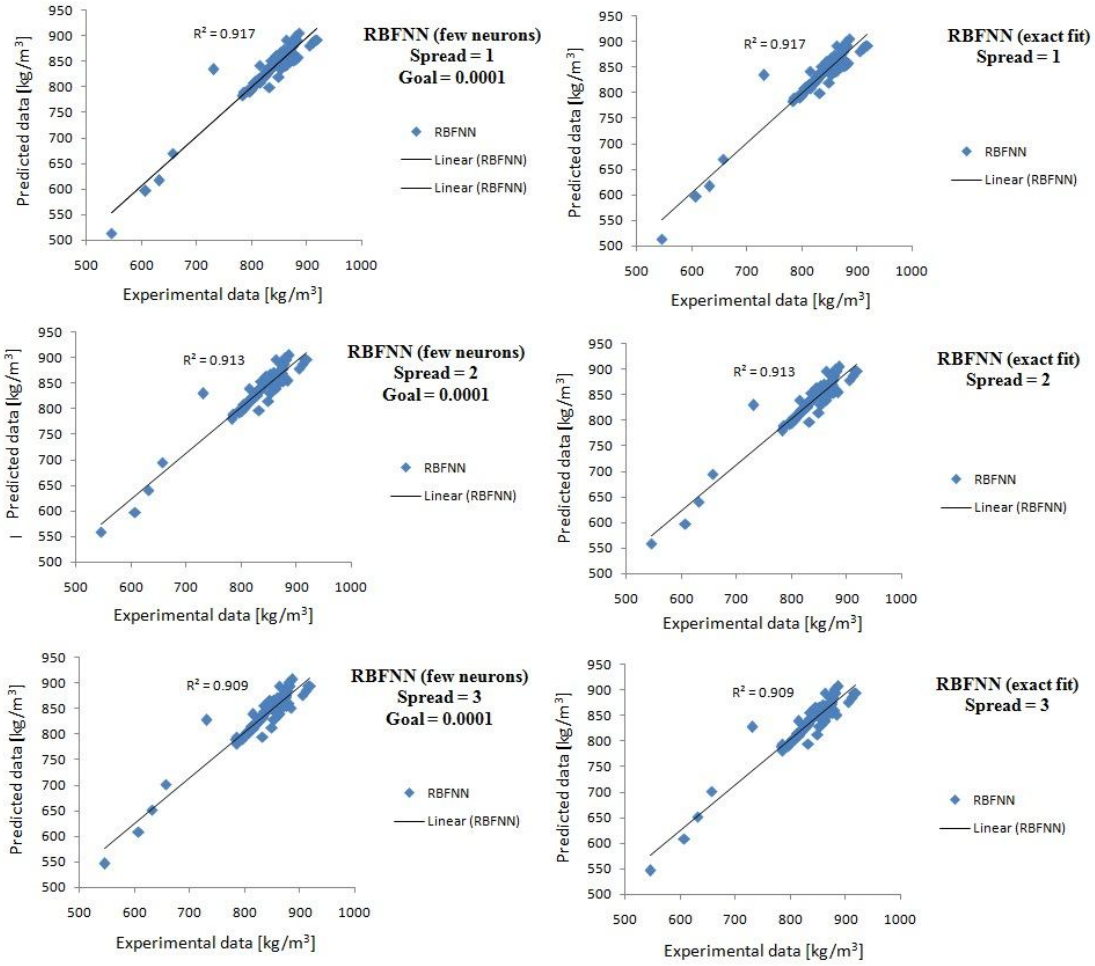

Figure 4.12: Fitting of the predicted of two approaches of RBFNN and experimental values for density of biodiesel blends using

Table 4.8: Radial Basis Function Neural Network configuration for the training and testing

Training					
RBFNN (few neurons)				**RBFNN(exact fit)**	
Spread	**Goals**	**Neurons**	**MSE**	**Spread**	**MSE**
1	0.0001	363	0.001982	1	0.001983
2	0.0001	363	0.00208	2	0.00209
3	0.0001	363	0.002123	3	0.002130
Testing					
RBFNN (few neurons)				**RBFNN(exact fit)**	
Spread	**Goals**	**Neurons**	R^2	**Spread**	R^2
1	0.0001	363	0.917	1	0.917
2	0.0001	363	0.913	2	0.913
3	0.0001	363	0.909	3	0.909

4.1.2 Modeling of Density of Biodiesel Blends using RBFNN

The test values obtained from the RBFNN model results were compared with experimental values as shown in Table 4.9. As a result, the test values obtained from RBFNN model were closed to experimental values of biodiesel blends density. Moreover, the maximum absolute relative error is approximately 4% which assigned a good agreement between the experimental and predicting values.

Table 4.9: Comparative study between experimental and RBFNN results of biodiesel density

Temperature [□]	Biodiesel fraction	Diesel fraction	Density [kg/m^3]		Absolute error [%]
			EXP	RBNN	
10	0.5	0.5	829.50	857.11	3.33
	1	0	865.80	856.26	1.10
15	0.5	0.5	884.00	858.37	2.90
	0.2	0.8	860.25	841.69	2.16
	1	0	817.57	828.01	1.28
	0.1	0.9	879.65	850.88	3.27
20	0.01	0.99	834.90	835.51	0.07
	0.25	0.75	832.25	836.66	0.53
	1	0	852.00	842.80	1.08
	0.6	0.4	783.10	760.12	2.93
	0	1	857.94	834.65	2.71
25	0.2	0.8	833.50	834.18	0.08
30	1	0	877.68	886.34	0.99
	0.25	0.75	825.13	830.74	0.68
	0.01	0.99	827.80	825.24	0.31
	0.5	0.5	826.15	846.74	2.49
	0.75	0.25	834.40	862.17	3.33
35	0.2	0.8	857.00	826.61	3.55
40	1	0	874.96	880.52	0.64
	0.5	0.5	837.41	837.44	0.00
	0.1	0.9	825.60	820.65	0.60
50	0.4	0.6	827.00	825.94	0.13
	0.2	0.8	816.50	817.74	0.15
	1	0	631.52	673.51	6.65
	0.8	0.2	879.80	847.85	3.63
	0.25	0.75	785.63	819.24	4.28
55	0.2	0.8	860.65	814.83	5.32
60	0.01	0.99	806.80	808.03	0.15
	0	1	806.20	809.38	0.39
	0.2	0.8	810.00	811.71	0.21
	1	0	848.90	866.05	2.02
	0.6	0.4	832.50	833.36	0.10
65	0.2	0.8	805.15	808.18	0.38
70	0.6	0.4	825.00	826.24	0.15
	0.4	0.6	813.50	802.38	1.37
	0.8	0.2	859.50	832.25	3.17
	1	0	812.14	859.33	5.81

Table 4.9: Continued

Temperature [□]	Biodiesel fraction	Diesel fraction	Density [kg/m^3]		Absolute error [%]
			EXP	RBFNN	
80	0.8	0.2	826.50	825.88	0.07
	0.2	0.8	796.50	796.23	0.03
	0.15	0.85	871.77	894.45	2.60
	1	0	841.29	854.23	1.54
85	0.1	0.9	831.50	790.05	4.99
90	0.2	0.8	795.10	789.79	0.67
	0	1	785.00	785.81	0.10
	0.6	0.4	815.70	808.00	0.94
	1	0	882.42	850.66	3.60
100	1	0	836.30	847.43	1.33
	0.1	0.9	799.60	783.67	1.99
120	1	0	850.08	834.21	1.87
130	1	0	815.00	820.14	0.63
140	1	0	845.05	859.35	1.69
180	1	0	656.85	669.69	1.95
200	1	0	886.43	880.52	0.67
220	1	0	606.93	595.96	1.81
280	1	0	545.25	523.85	3.92

4.4 Response Surface Methodology Model of Density of Biodiesel Blends

The effect of temperature and volume fraction of biodiesel blends with petro-diesel on the density of biodiesel blends was tested using RSM. The experimental runs were randomized to minimize the effects of unexpected variability in the observed responses. The methodology adopted allows the formulation of a polynomial equation, which describes the process. This study tested several degrees of polynomial equation for two independent variables (temperature (T) and volume fraction of biodiesel (*w*)) and topologies for the estimation and prediction of density of biodiesel. Therefore, Table 4.10 presents the best degree of polynomial equation.

Table 4.10: The effect of different order of polynomial equation of density and topologies on R^2, SSE and RSME

Degrees		R-square (R^2)	Squared standard error (SSE)	Root mean squared error (RSME)
x-data (*w*) [%]	y-data (T) [K]			
3	2	0.9599	5.83E04	11.45
3	1	0.9717	4.122E04	9.603
4	1	0.9613	5.63E04	11.25
4	4	0.951	7.13E04	12.74
2	1	0.9663	4.911E04	10.46

A series of topologies was examined in order to determine the optimum number of degree of independent variables and these values were varied from 2 to 4. Besides, R^2, SSE and RSME were used as a measure of predictive ability of the equation. Hence, the best topology i.e. degree of 3 for volume fraction of biodiesel blends and degree of 1 for temperature was chosen (Table 4.11) due to the values of R^2. Each response was used to develop a mathematical model that correlates the kinematic viscosities to the independent reaction variables via polynomial equation as given below:

$$\rho(w,T) = p_{00} + p_{10}w + p_{01}T + p_{20}w^2 + p_{11}wT + p_{30}w^3 + p_{21}w^2T \qquad (6.1)$$

where *w* is normalized by mean 0.6185 and std (standard) 0.3712, *T* is normalized by mean 333.8 and std 45.54 and $p_{00}, p_{10}, p_{01}, p_{20}, p_{11}, p_{30}$ and p_{21} are polynomial coefficients (Table 4.11).

Table 4.11: Polynomial equation coefficients for kinematic viscosity of biodiesel blends

Polynomial equation coefficients	Value Eq. (6.1)
p_{00}	*832.3*
p_{10}	*23.52*
p_{01}	*27.47*
p_{20}	49.57
p_{11}	*-1.786*
p_{30}	*-3.395*
p_{21}	*-3.884*

Due to interaction effects between the variables, the parameters could not be analyzed independently. The significance of the parameters in the model was obtained using Matlab 2013b toolbox. The contour plots and surface view (3D) of the density of biodiesel blends shown in Figure 4 which indicate the interaction effects in a polynomial equation (Eq. 6.1). The contour areas help to explain how the density of biodiesel blends varies with a change in the temperature and volume fraction of biodiesel. Moreover, the contour plots are useful tools for identifying the optimum operating conditions and related response values. The points on each contour and surface view area indicate the density value of biodiesel in the specified temperature and volume fraction of biodiesel. The residual indicates the difference between the predicted data and actual data of the density of biodiesel blends.

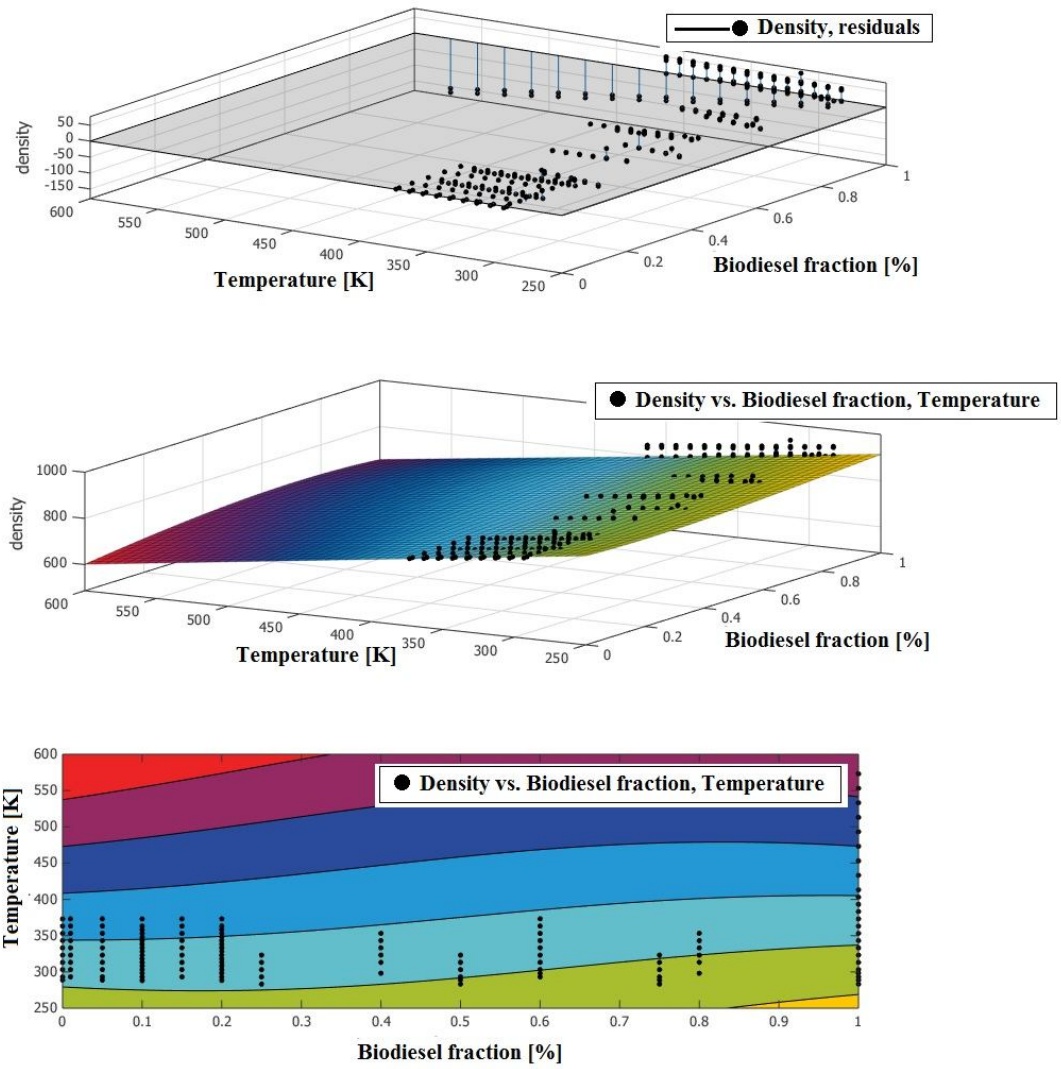

Figure 4.13: surface view of density using Eq. (6.1)

4.5 Adaptive Neuro–Fuzzy Inference System (ANFIS) Model of Kinematic Viscosity

4.5.1 Method of Applications of ANFIS for Kinematic Viscosity of Biodiesels

The proposed ANFIS methodology to predict the kinematic viscosity of biodiesel blends using various biodiesel obtained from vegetable oils or waste vegetable oils. The developed ANFIS model for predicting the kinematic viscosity at different temperature and volume fraction of petro-diesel is shown in Figure 4.14. The model was trained with part

of the database derived from the experimental results of literature studies. A total of 934 experimental points were obtained from various scientific publications to estimate the kinematic viscosity of biodiesel blends. The database was first split into training data (80%) and testing data (20%). The training data set was also split into two parts, a training set (60%) and a checking set (20%).

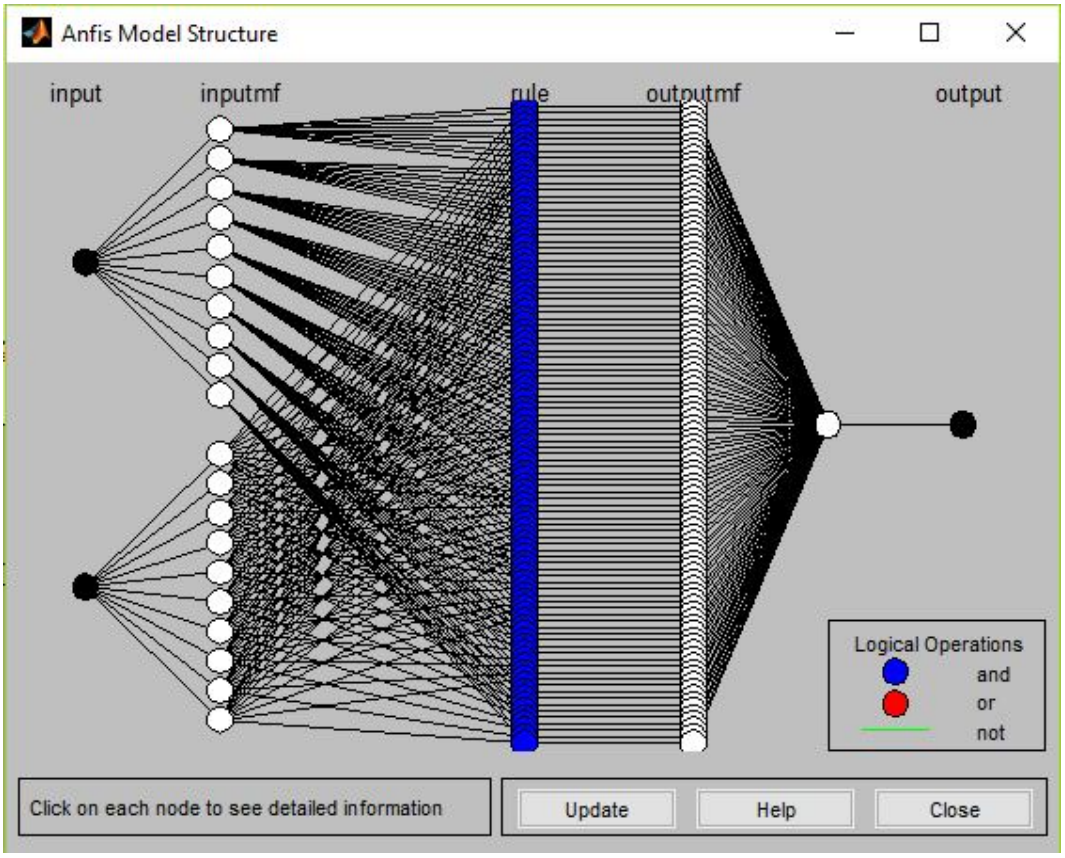

Figure 4.14: ANFIS architecture for predicting kinematic viscosity of biodiesel blends

In this work, the best number of membership functions for each input was determined as 3, the membership grades takes the Gaussian-shaped membership functions and the output part of each rule uses a constant defuzzifier formula, which found by trial and error methods (Table 4.12 and Table 4.13). Moreover, two methods (hybrid and back-propagation) are tested for generation ANFIS that the results is obtained in Tables 4.1 and

4.3. The results show the training error in the hybrid method is lower of back-propagation method. Therefore, the hybrid method has used for this study. Table 4.14 shows the numbers of the system parameters of ANFIS model for kinematic viscosity of biodiesel blends.

Table 4.12. The ANFIS information by the hybrid optimum method

Optimum Method	Number of MF	MF type	MF type (output)	Training error	Testing error
Hybrid	2	Gaussmf	Constant	0.0809	0.03307
Hybrid	3	Gaussmf	Constant	0.0802	0.0348
Hybrid	4	Gaussmf	Constant	0.08127	0.0386
Hybrid	5	Gaussmf	Constant	0.0809	0.0371
Hybrid	6	Gaussmf	Constant	0.0806	00376
Hybrid	7	Gaussmf	Constant	0.0803	0.036
Hybrid	8	Gaussmf	Constant	0.08	0.0367
Hybrid	9	Gaussmf	Constant	0.0801	0.0365
Hybrid	10	Gaussmf	Constant	0.0798	0.036
Hybrid	11	Gaussmf	Constant	0.0803	0.038
Hybrid	10	Gaussmf	Linear	0.0801	0.0365

Table 4.13. The ANFIS information by the back-propagation optimum method

Optimum Method	Number of MF	MF type	MF type (output)	Training error	Testing error
back-propagation	2	Gaussmf	Constant	0.0821	0.0348
back-propagation	3	Gaussmf	Constant	0.0815	0.0341
back-propagation	10	Gaussmf	Constant	0.0811	0.0361
back-propagation	10	Gaussmf	Linear	0.0817	0.0371

Table 4.14: System parameters of the ANFIS model

ANFIS model parameters	
Number of nodes	245
Number of linear parameters	100
Number of nonlinear parameters	40
Total number of parameters	140
Number of training data pairs	560
Number of checking data pairs	187
Number of fuzzy rules	100

Table 4.15 summarized the ANFIS information and errors which used in this study for predicting the kinematic viscosity of biodiesel blends. The ANFIS network was able to achieve training and checking the lowest RMSE (root mean standard error) for kinematic viscosity of biodiesel blends as shown in Figure 4.15

Table 4.15: The ANFIS information used in the predicting kinematic viscosity of biodiesel by the hybrid optimum method

Biodiesel blend with Diesel	
Epoch	1000
RMSE	
Training error	0.0798
Tasting error	0.0374
Checking error	0.0529

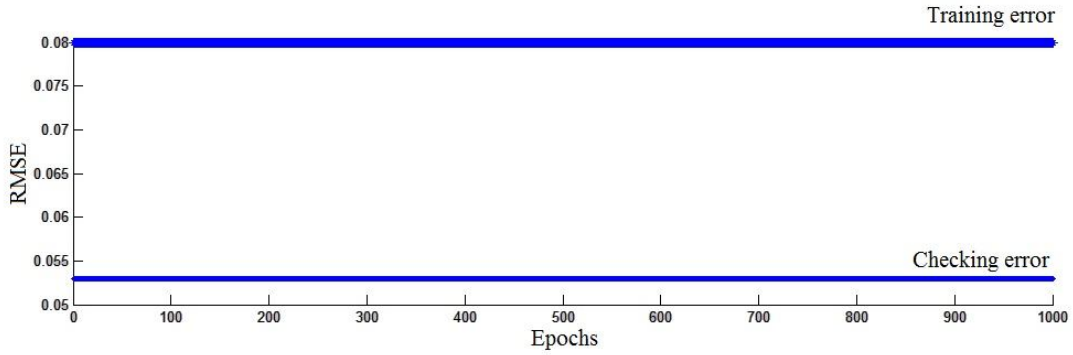

Figure 4.15: Training and checking RMSE achieve with ANFIS for kinematic viscosity of biodiesel blends

Figure 4.16 indicates rule viewers of kinematic viscosity that shows value of the various inputs to the ANFIS models and computed output. The kinematic viscosity (output) can be predicted by varying the input parameters, including temperature and volume fraction of biodiesel to the developed ANFIS model.

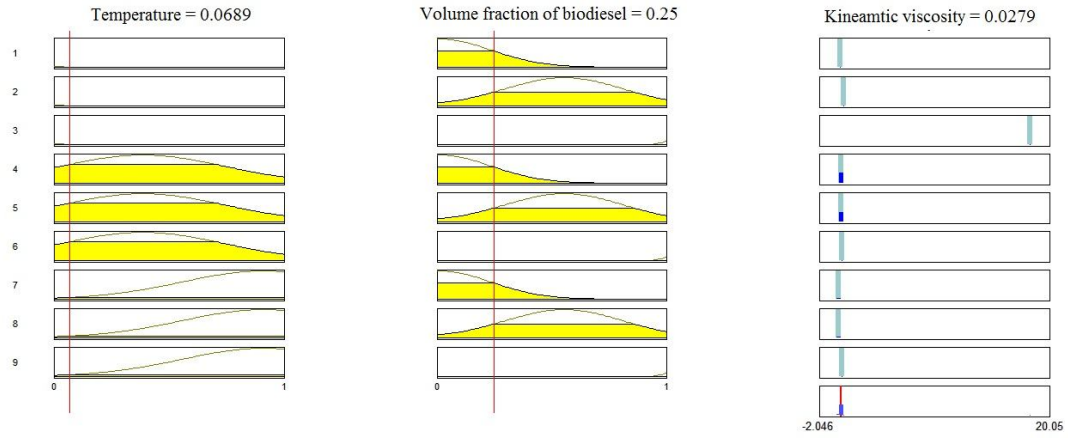

Figure 4.16: Rule viewer of ANFIS model for density of biodiesel blends

The 3D surface plots of kinematic viscosity of biodiesel blend with benzene against temperature and volume fraction of biodiesel is depicted in Figure 4.17 The plot suggest strong interaction between the variables with significant influence on the kinematic viscosity of biodiesel blends. From the Figure, increasing in volume fraction of biodiesel

leads to increase the kinematic viscosity of biodiesel blends, while the highest temperature leads to decrease the kinematic viscosity of biodiesel blends as shown in Figure 4.17.

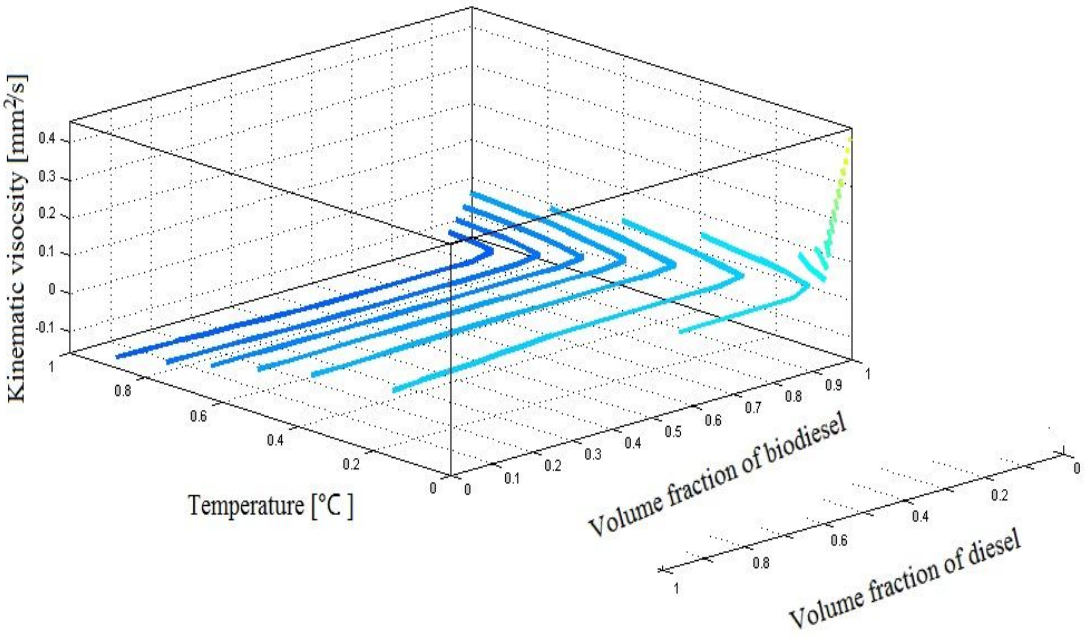

Figure 4.17: Surface viewer of ANFIS model for kinematic viscosity of biodiesel blends

4.5.2 Modeling of Kinematic Viscosity of Biodiesel Blends using ANFIS

Figure 4.18 illustrates the results of fitting the predicted and experimental values for kinematic viscosity of biodiesel blends, using linear regression. It can be seen that these values are close to unity highlighting proper fitting of the predicted values by the adopted methodology. Additionally, Table 4.16 shows the comparison between the experimental results with predicted data using ANFIS. It can be noticed that the experimental results and the data obtained by ANFIS are very close to each other. Moreover, the maximum absolute relative error between these values is about 19%, which indicate an excellent agreement between the experimental and predicting values.

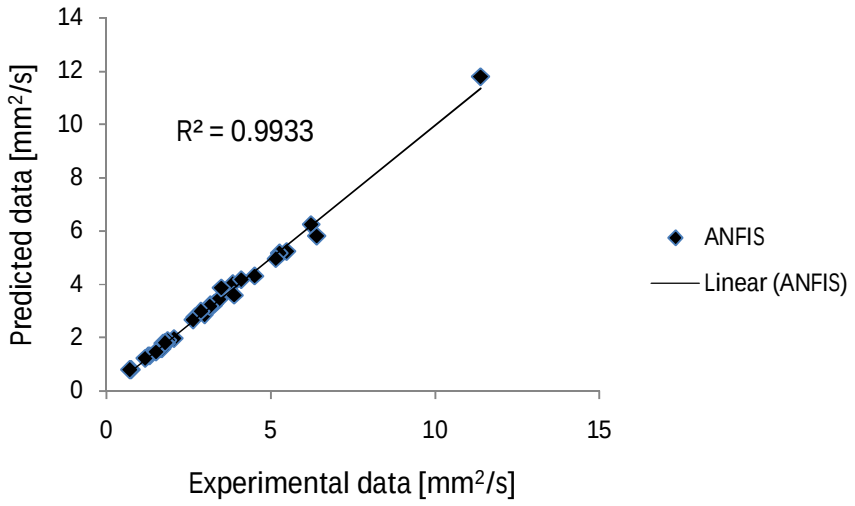

Figure 4.18: Fitting of the predicted ANFIS and experimental values for kinematic viscosity of biodiesel blends

Table 4.16: Comparative study between experimental and ANFIS results of kinematic viscosity of biodiesel

Temperature [□]	Biodiesel fraction	Diesel fraction	Kinematic viscosity [mm^2/s]		Absolute error [%]
			EXP	ANFIS	
10	0.5	0.5	4.51	4.30	4.59
	0.25	0.75	3.25	3.20	1.54
20	0.6	0.4	6.23	6.23	0.06
	0.65	0.35	6.40	5.80	9.38
25	0.5	0.5	5.49	5.22	4.88
30	0.7	0.3	5.26	5.17	1.79
	0.1	0.9	3.29	3.27	0.64
	0.65	0.35	5.16	4.95	4.11
35	0.1	0.9	3.16	3.21	1.64
40	0.6	0.4	3.84	4.01	4.42
	0.65	0.35	4.11	4.16	1.28
	0.45	0.55	3.89	3.58	7.76
	0.5	0.5	3.42	3.42	0.11
45	0.2	0.8	2.70	2.77	2.54
50	0.35	0.65	2.99	2.85	4.55
	0.75	0.25	2.63	2.65	0.61
	0.9	0.1	3.50	3.85	10.03
	0.55	0.45	3.14	3.17	0.78
60	0.75	0.25	2.88	2.98	3.47
70	0.4	0.6	2.06	1.95	5.22
	0.1	0.9	1.80	1.79	0.56
	0.15	0.85	1.87	1.88	0.79
	0.05	0.95	1.72	1.77	2.84
80	1	0	11.39	11.78	3.42
	0.15	0.85	1.63	1.57	3.94
	0.4	0.6	1.83	1.78	2.52
100	0.25	0.75	1.28	1.31	2.34
	0.2	0.8	1.32	1.30	1.17
	1	0	1.69	1.58	6.51
	0.05	0.95	1.18	1.21	2.40
110	1	0	1.51	1.45	3.97
120	1	0	1.79	1.80	0.67
260	1	0	0.75	0.79	5.90
280	1	0	0.71	0.79	10.80

4.6 Artificial Neural Network (ANN) Model of Kinematic Viscosity

4.6.1 Method of Applications of ANN for Kinematic Viscosity of Biodiesels

The kinematic viscosity of biodiesel blends was estimated considering an input layer with two independent variables (temperature and volume fraction of biodiesel) eight neurons in the four hidden layer, as well as one response variable in the output layer (kinematic viscosity), which made an architecture of 2:4:1 as shown in Figure 4.19. Approximately 80% of the experimental data was used for training, while the remaining 20% was reserved for testing. The observed experimental data were normalized for improving the performance of the network. The back propagation algorithm was used for training the ANN model.

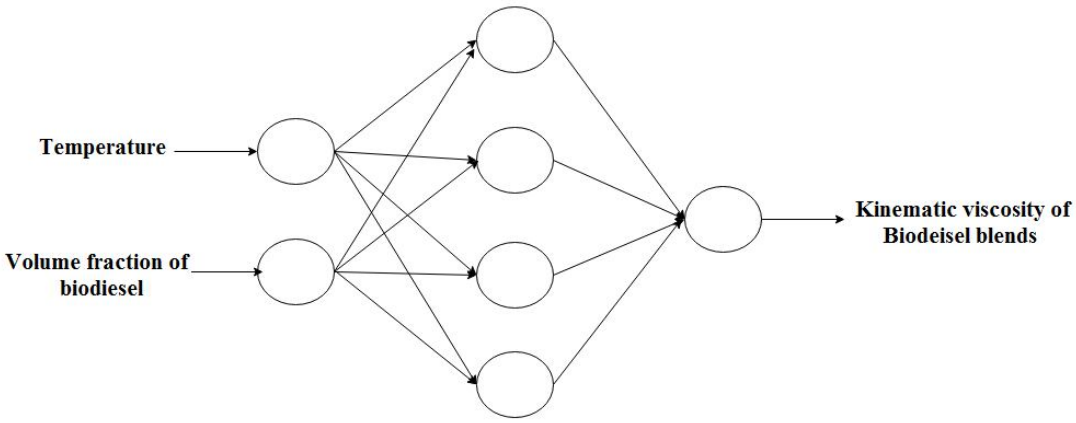

Figure 4.19: Schematic representation of ANN for predicting kinematic viscosity

The performance of ANN model is noticeably affected by the number of hidden layers and number of neurons in each hidden layer. The optimum number of neurons in the hidden layer was selected as 4. The maximum number of epochs and goal were fixed as 1000 and 0.000001, respectively, during the training. For the chosen network the training performance is achieved with minimum error of 8.6581×10^{-6} error rate, which is shown in Figure 4.20.

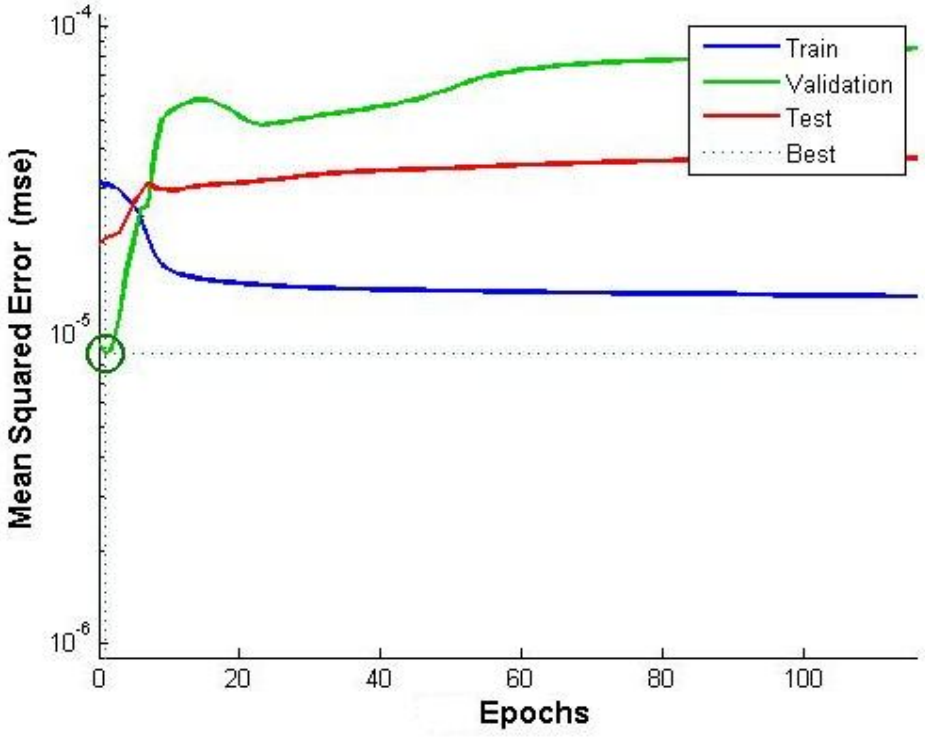

Figure 4.20: Performance graph of tested ANN model

A linear relation for the training, validation, testing and performance of the network with high correlation coefficients (R) of kinematic viscosity of biodiesel blends is shown in Figure 4.21. The high coefficients of correlation (R) obtained during the training, validation and testing of the kinematic viscosity network display very good relationship between the output and the experimental values of kinematic viscosity.

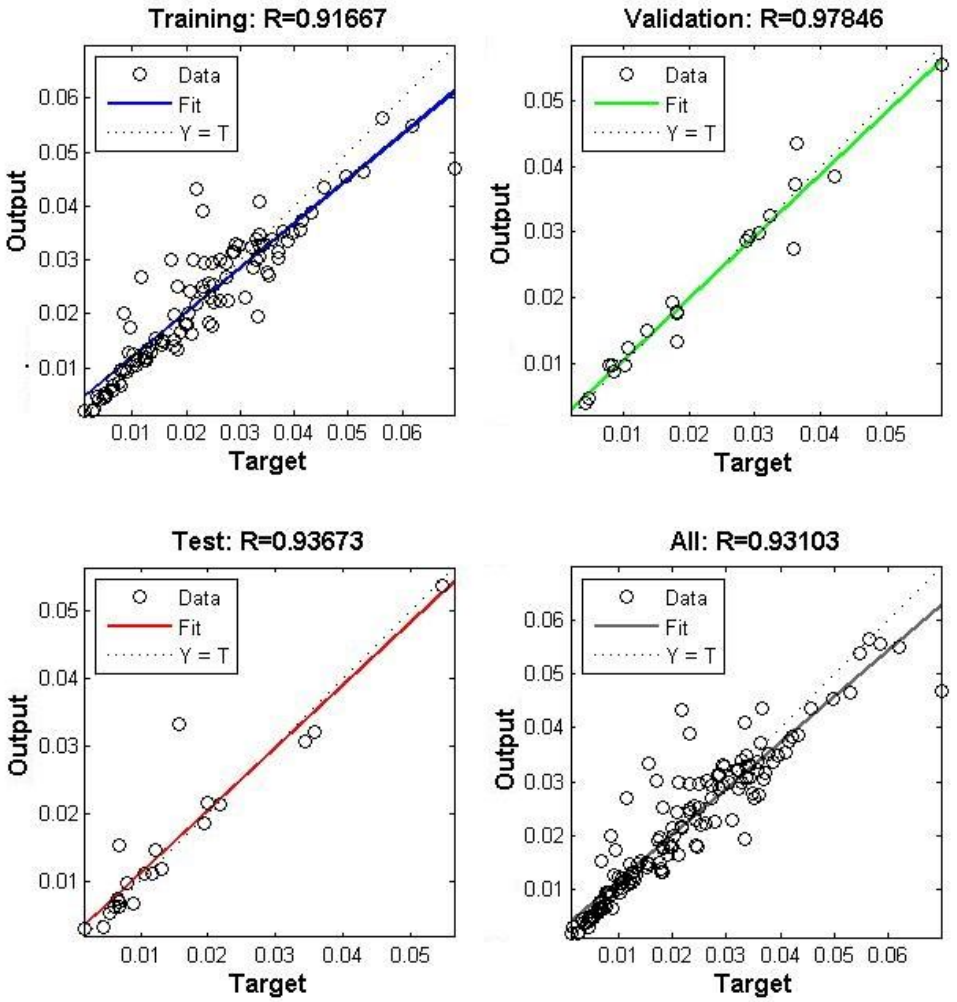

Figure 4.21: Regression plots for density of biodiesel blends network

4.6.2 Modeling of Kinematic Viscosity of Biodiesel Blends using AN N

The results of fitting the predicted and experimental values for kinematic viscosity of biodiesel blends, using linear regression is shown in Figure 4.22. It can be seen that these values are close to unity highlighting proper fitting of the predicted values by the adopted methodology. In addition, Table 4.17 demonstrates the testing results of kinematic viscosity using ANN model. Also, it shows the comparison between the experimental results with predicted data of kinematic viscosity of biodiesel blends. It can be noticed that the experimental results and the data obtained using ANN are very close to each other.

Furthermore, the maximum absolute relative error obtained is about 19%, which indicate an excellent agreement between the experimental and predicting values as shown in Table 4.17.

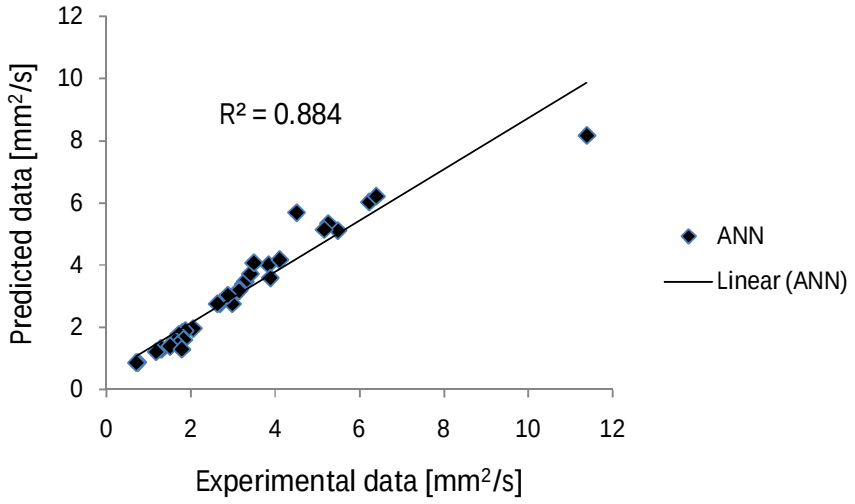

Figure 4.22: Fitting of the predicted ANN and experimental values for kinematic viscosity of biodiesel blends

Table 4.17: Comparative study between experimental and ANN results of kinematic viscosity of biodiesel

Temperature [□]	Biodiesel fraction	Diesel fraction	Kinematic viscosity [mm^2/s]		Absolute error [%]
			EXP	ANN	
10	0.5	0.5	4.51	5.68	25.99
	0.25	0.75	3.25	3.39	4.41
20	0.6	0.4	6.23	6.02	3.38
	0.65	0.35	6.40	6.21	2.98
25	0.5	0.5	5.49	5.11	6.97
30	0.7	0.3	5.26	5.33	1.26
	0.1	0.9	3.29	3.47	5.47
	0.65	0.35	5.16	5.14	0.43
35	0.1	0.9	3.16	3.21	1.64
40	0.6	0.4	3.84	4.01	4.42
	0.65	0.35	4.11	4.16	1.28
	0.45	0.55	3.89	3.58	7.76
40	0.5	0.5	3.42	3.72	8.87
45	0.2	0.8	2.70	2.77	2.54
50	0.35	0.65	2.99	2.75	7.83
	0.75	0.25	2.63	2.75	4.42
	0.9	0.1	3.50	4.07	16.23
	0.55	0.45	3.14	3.17	0.78
60	0.75	0.25	2.88	3.03	5.07
70	0.4	0.6	2.06	1.95	5.22
	0.1	0.9	1.80	1.83	1.54
	0.15	0.85	1.87	1.88	0.79
	0.05	0.95	1.72	1.77	2.84
80	1	0	11.39	8.17	28.31
	0.15	0.85	1.63	1.57	3.94
	0.4	0.6	1.83	1.60	12.45
100	0.25	0.75	1.28	1.30	1.92
	0.2	0.8	1.32	1.30	1.17
	1	0	1.69	1.44	14.93
	0.05	0.95	1.18	1.21	2.40
110	1	0	1.51	1.39	8.14
120	1	0	1.79	1.29	27.94
260	1	0	0.75	0.86	15.89
280	1	0	0.71	0.86	20.13

4.7 Radial Basis Function Neural Network Model of Kinematic Viscosity

4.7.1 Method of Applications of RBFNN for Kinematic Viscosity of Biodiesels

Training of the first approach was stopped when either of the performance goals was reached. Training of the network has been done with different number of RBF units. For various values of spread (unit) the network error was analyzed it was observed that for a spread of 1, the error was minimum. The network was trained with optimum number of centers determined from the random selection method and a spread of 1. Results for the various performances of the RBFNN are presented in Table 4.18. It can be seen that it can be observed that minimum mean squared error (MSE) of RBFNN training results is equal to 3.64×10^{-5} obtained when spread number is equal to 11 units.

Table 4.18: Radial Basis Function Neural Network configuration for the kinematic viscosity training

Spread	Neurons	Goal	MSE
1	143	1 E-7	5.81E-05
2	143	1 E-7	5.29E-05
3	143	1 E-7	5.26E-05
4	143	1 E-7	5.25E-05
5	143	1 E-7	5.15E-05
6	143	1 E-7	4.90E-05
7	143	1 E-7	4.75E-05
8	143	1 E-7	4.55E-05
9	143	1 E-7	4.05E-05
10	143	1 E-7	3.66E-05
11	143	1 E-7	3.64E-05
12	143	1 E-7	3.67E-05
13	143	1 E-7	3.85E-05
14	143	1 E-7	3.95E-05
15	143	1 E-7	4.05E-05

4.7.2 Modeling of Kinematic Viscosity of Biodiesel Blends using RBFNN

Figure 4.22 shows the results of fitting the predicted and experimental values for kinematic viscosity of biodiesel blends. It can be seen that predicted data are too closed to the experimental data. The test values obtained from the RBFNN model results were compared with experimental values as shown in Table 4.19. As a result, the test values obtained from RBFNN model were closed to experimental values of biodiesel blends density. Moreover, the maximum absolute relative error is approximately 42% which assigned a good agreement between the experimental and predicting values.

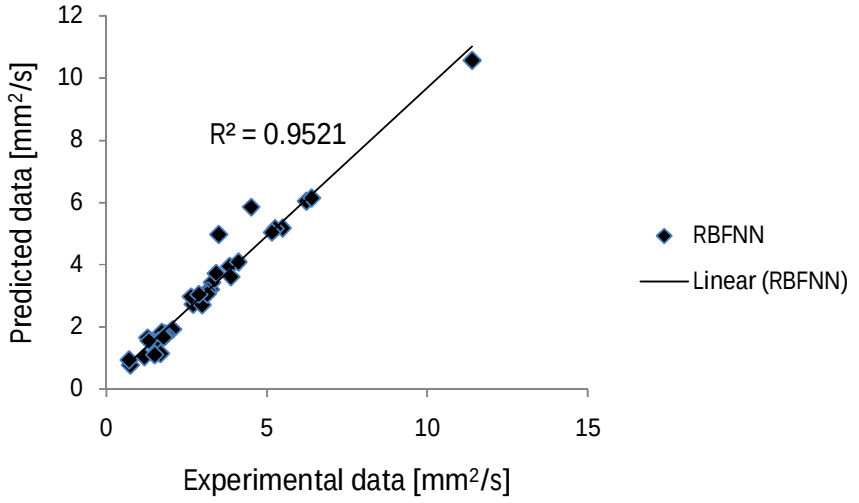

Figure 4.22: Fitting of the predicted RBFNN and experimental values for kinematic viscosity of biodiesel blends

Table 4.19: Comparative study between experimental and RBFNN results of kinematic viscosity of biodiesel

Temperature [□]	Biodiesel fraction	Diesel fraction	Kinematic viscosity [mm^2/s]		Absolute error [%]
			EXP	RBFNN	
10	0.5	0.5	4.51	5.84	29.69
	0.25	0.75	3.25	3.21	1.18
20	0.6	0.4	6.23	6.04	3.19
	0.65	0.35	6.40	6.14	4.00
25	0.5	0.5	5.49	5.17	5.71
30	0.7	0.3	5.26	5.16	1.92
	0.1	0.9	3.29	3.44	4.40
	0.65	0.35	5.16	5.04	2.44
35	0.1	0.9	3.16	3.16	0.06
40	0.6	0.4	3.84	3.95	2.87
	0.65	0.35	4.11	4.08	0.70
	0.45	0.55	3.89	3.60	7.28
	0.5	0.5	3.42	3.72	9.00
45	0.2	0.8	2.70	2.72	0.65
50	0.35	0.65	2.99	2.71	9.37
	0.75	0.25	2.63	2.97	12.67
	0.9	0.1	3.50	4.97	42.12
	0.55	0.45	3.14	3.06	2.71
60	0.75	0.25	2.88	3.04	5.68
70	0.4	0.6	2.06	1.91	7.16
	0.1	0.9	1.80	1.78	1.14
	0.15	0.85	1.87	1.77	5.54
	0.05	0.95	1.72	1.83	6.40
80	1	0	11.39	10.57	7.22
	0.15	0.85	1.63	1.57	3.89
	0.4	0.6	1.83	1.69	7.29
100	0.25	0.75	1.28	1.65	28.78
	0.2	0.8	1.32	1.54	16.92
	1	0	1.69	1.14	32.65
	0.05	0.95	1.18	1.03	12.38
110	1	0	1.51	1.10	26.84
120	1	0	1.79	1.66	6.99
260	1	0	0.75	0.76	2.16
280	1	0	0.71	0.93	30.81

4.8 Response Surface Methodology Model of Kinematic Viscosity

The influence of temperature and volume fraction of biodiesel blends with petro-diesel on the kinematic viscosity of biodiesel blends was tested using RSM. The experimental runs were randomized to minimize the effects of unexpected variability in the observed responses. The methodology adopted allows the formulation of a polynomial equation, which describes the process. This study tested several degrees of polynomial equation for two independent variables (temperature (T) and volume fraction of biodiesel (*w*)) and topologies for the estimation and prediction of kinematic viscosity of biodiesel. Therefore, Table 4.20 presents the best degree of polynomial equation.

Table 4.20: The effect of different order of polynomial equation and topologies on R^2, SSE and RSME

Degrees				
x-data (*w*) [%]	**y-data (T) [K]**	**R-square (R^2)**	**Squared standard error (SSE)**	**Root mean squared error (RSME)**
1	1	0.7883	143.7	0.7675
2	1	0.8365	111.013	0.6773
3	1	0.8019	134.51	0.7486
4	1	0.8054	132.164	0.7452
4	2	0.9027	66.07	0.5302

A series of topologies was examined in order to determine the optimum number of degree of independent variables and these values were varied from 1 to 4. Besides, R^2, SSE and RSME were used as a measure of predictive ability of the equation. Hence, the best topology i.e. degree of 4 for volume fraction of biodiesel blends and degree of 2 for temperature was chosen (Table 4.20) due to the values of R^2. Each response was used to develop a mathematical model that correlates the kinematic viscosities to the independent reaction variables via polynomial equation as given below:

$$\nu(w,T) = p_{00} + p_{10}w + p_{01}T + p_{20}w^2 + p_{11}wT + p_{02}T^2 + p_{12}wT^2 + p_{30}w^3 + p_{21}w^2T + p_{40}w^4 + p_{31}w^3T + p_{22}w^2T^2 \quad (6.2)$$

$$\nu(w,T) = p_{00} + p_{10}w + p_{01}T + p_{20}w^2 + p_{11}wT \quad (6.3)$$

where, $p_{00}, p_{10}, p_{01}, p_{20}, p_{11}, p_{02}, p_{30}, p_{21}, p_{12}, p_{40}, p_{31}$ and $p_{22}$are polynomial coefficients (Table 4.21).

Table 4.21: Polynomial equation coefficients for kinematic viscosity of biodiesel blends

Polynomial equation coefficients	Value	
	Eq. (6.2)	**Eq. (6.3)**
p_{00}	46.81	13.6
p_{10}	-12.67	15.24
p_{01}	-0.2384	-0.03456
p_{20}	49.57	-0.7883
p_{11}	0.08945	-0.0381
p_{02}	0.0003112	0.00
p_{30}	-39.96	0.00
p_{21}	-0.1505	0.00
p_{12}	-0.0001405	0.00
p_{40}	-5.819	0.00
p_{31}	0.1407	0.00
p_{22}	-3.146E-06	0.00

Due to interaction effects between the variables, the parameters could not be analyzed independently. The significance of the parameters in the model was obtained using Matlab 2013b toolbox. The contour plots and surface view (3D) of the density of biodiesel blends shown in Figure 4.25 and 4.26 which indicate the interaction effects in a polynomial equation Eq. 6.2 and 6.3, respectively. The contour areas help to explain how the density of biodiesel blends varies with a change in the temperature and volume fraction of biodiesel. Moreover, the contour plots are useful tools for identifying the optimum operating

conditions and related response values. The points on each contour and surface view area indicate the density value of biodiesel in the specified temperature and volume fraction of biodiesel. The residual indicates the difference between the predicted data and actual data of the kinematic visocsity of biodiesel blends.

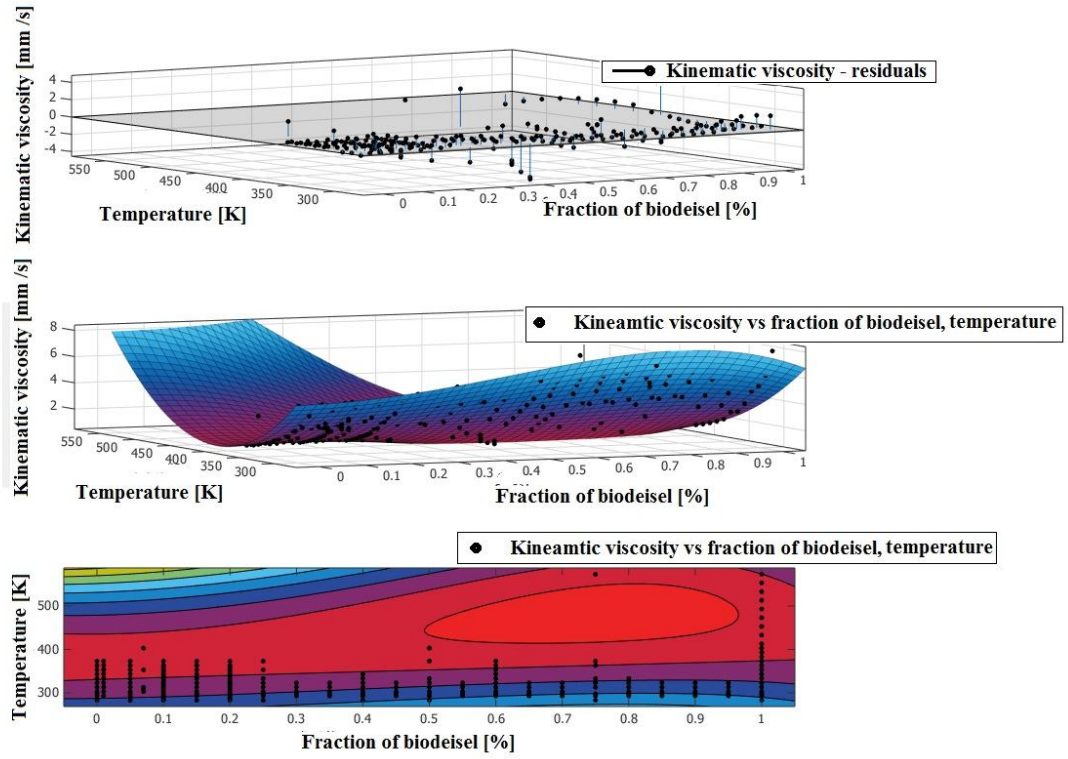

Figure 4.25: surface view of kinematic viscosity using Eq. (6.2)

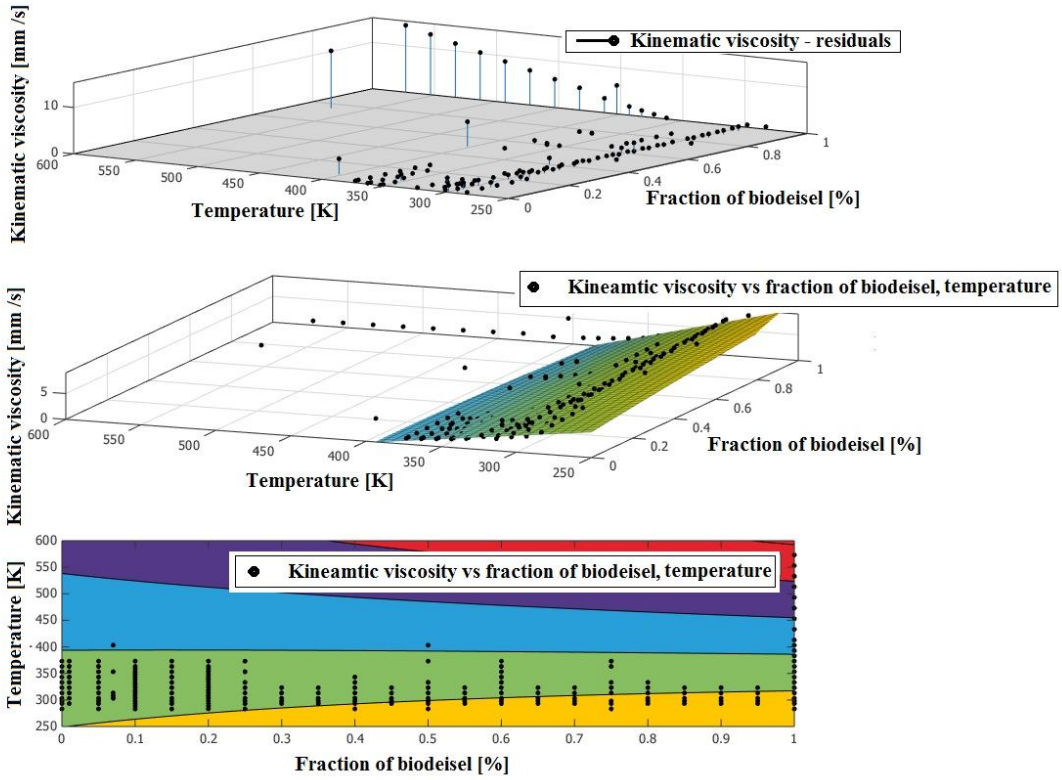

Figure 4.26: surface view of kinematic viscosity using Eq. (6.3)

The correlation model prediction error for kinematic viscosity is illustrated in Figure 4.27. It is observed that both the individual single variable (only temperature dependent) model and the two-variable (temperature and biodiesel fraction) models for kinematic viscosity prediction has excellent agreement with the experimental results. The predicted data for kinematic viscosity are within 0 – 15 low relative error of the experimental data at 280 to 400K.

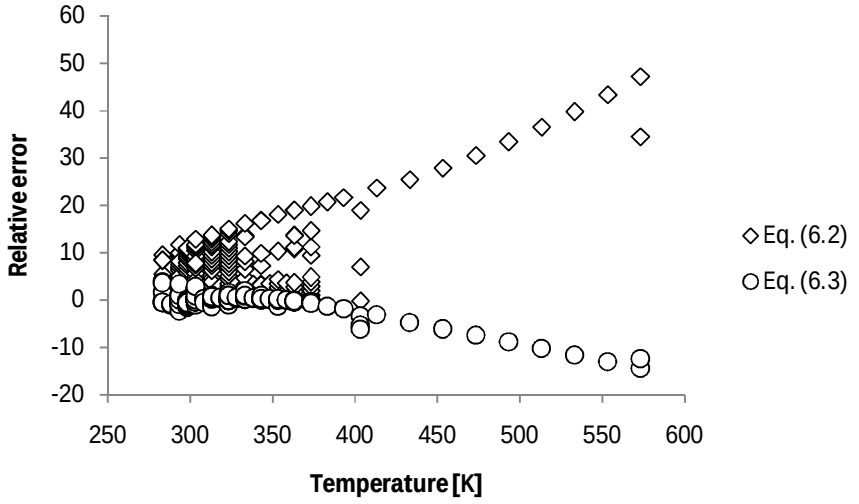

Figure 4.27: Relative error between experiments data and predicted data using RSM

4.9 Comparing between ANFIS, ANN and RBF approaches

Figures 4.28 and 4.29 show a comparison for the calculated density and kinematic viscosity data using ANFIS, ANN and RBFNN approaches expressed by their percent absolute error, the results are in the range of 0.2% to 3%, 0.2% to 5%, and 0 % to 6%, for predicted density data using ANFIS, ANN and RBFNN, respectively. Moreover, the results of kinematic viscosity using ANFIS, ANN and RBFNN are in the range of 0% to 10%, 0.7% to 25%, and 0.7 % to 30%, respectively as shown in Figure 4.28 and tabulated in Table 4.23. Figures 4.28 and 4.29 and Tables 4.22 and 4.23 indicate that ANFIS approach gives an excellent agreement between the experimental and predicting values of density and kinematic viscosity of biodiesel.

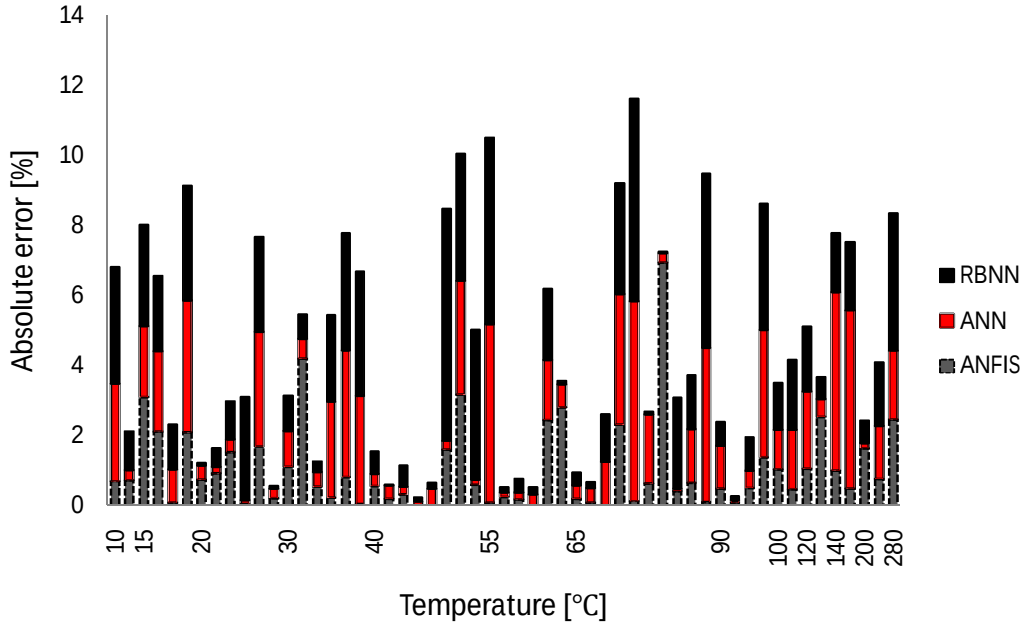

Figure 4.28: Absolute error vs temperature for 3 models for predicting density of biodiesel

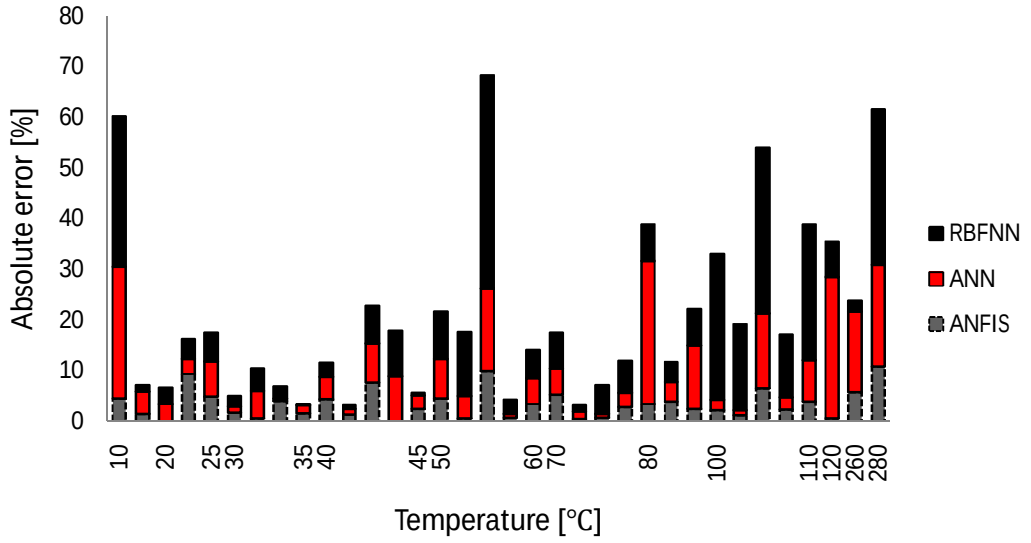

Figure 4.29: Absolute error vs temperature for 3 models for predicting kinematic viscosity of biodiesel

Table 4.22: Evaluation of predictive models for the density of Biodiesel

T [℃]	Biodiesel fraction	Diesel fraction	Density [kg/m^3]				Absolute error [%]		
			EXP	ANFIS	ANN	RBNN	ANFIS	ANN	RBNN
10	0.5	0.5	829.50	835.29	852.68	857.11	0.70	2.79	3.33
	1	0	865.80	859.49	868.36	856.26	0.73	0.30	1.10
15	0.5	0.5	884.00	856.52	866.06	858.37	3.11	2.03	2.90
	0.2	0.8	860.25	842.08	840.46	841.69	2.11	2.30	2.16
	1	0	817.57	818.31	825.32	828.01	0.09	0.95	1.28
	0.1	0.9	879.65	898.12	846.38	850.88	2.10	3.78	3.27
20	0.01	0.99	834.90	841.23	831.64	835.51	0.76	0.39	0.07
	0.25	0.75	832.25	839.96	833.86	836.66	0.93	0.19	0.53
	1	0	852.00	865.01	855.26	842.80	1.53	0.38	1.08
	0.6	0.4	783.10	782.65	782.15	760.12	0.06	0.12	2.93
	0	1	857.94	843.36	829.82	834.65	1.70	3.28	2.71
25	0.2	0.8	833.50	835.29	835.80	834.18	0.21	0.28	0.08
30	1	0	877.68	887.50	886.77	886.34	1.12	1.04	0.99
	0.25	0.75	825.13	859.91	829.85	830.74	4.21	0.57	0.68
	0.01	0.99	827.80	832.32	824.31	825.24	0.55	0.42	0.31
	0.5	0.5	826.15	828.07	848.73	846.74	0.23	2.73	2.49
	0.75	0.25	834.40	841.23	864.78	862.17	0.82	3.64	3.33
35	0.2	0.8	857.00	856.52	830.47	826.61	0.06	3.10	3.55
40	1	0	874.96	879.86	877.99	880.52	0.56	0.35	0.64
	0.5	0.5	837.41	839.11	840.66	837.44	0.20	0.39	0.00
	0.1	0.9	825.60	822.98	827.52	820.65	0.32	0.23	0.60
50	0.4	0.6	827.00	826.80	826.27	825.94	0.02	0.09	0.13
	0.2	0.8	816.50	816.61	820.51	817.74	0.01	0.49	0.15
	1	0	631.52	641.72	633.00	673.51	1.62	0.23	6.65
	0.8	0.2	879.80	851.85	851.10	847.85	3.18	3.26	3.63
	0.25	0.75	785.63	790.29	784.39	819.24	0.59	0.16	4.28
55	0.2	0.8	860.65	859.91	816.61	814.83	0.09	5.12	5.32
60	0.01	0.99	806.80	804.73	805.84	808.03	0.26	0.12	0.15
	0	1	806.20	804.73	804.68	809.38	0.18	0.19	0.39
	0.2	0.8	810.00	809.82	812.46	811.71	0.02	0.30	0.21
	1	0	848.90	828.07	863.59	866.05	2.45	1.73	2.02
	0.6	0.4	832.50	808.97	827.09	833.36	2.83	0.65	0.10
65	0.2	0.8	805.15	806.85	808.09	808.18	0.21	0.37	0.38
70	0.6	0.4	825.00	824.25	821.47	826.24	0.09	0.43	0.15
	0.4	0.6	813.50	813.64	803.46	802.38	0.02	1.23	1.37
	0.8	0.2	859.50	839.54	827.45	832.25	2.32	3.73	3.17
	1	0	812.14	813.22	858.51	859.33	0.13	5.71	5.81

Table 4.22: Continued

T [□]	Biodiesel fraction	Diesel fraction	Density [kg/m^3]				Absolute error [%]		
			EXP	ANFIS	ANN	RBNN	ANFIS	ANN	RBNN
80	0.8	0.2	826.50	821.28	810.16	825.88	0.63	1.98	0.07
	0.2	0.8	796.50	851.85	794.35	796.23	6.95	0.27	0.03
	0.15	0.85	871.77	867.98	872.33	894.45	0.44	0.06	2.60
	1	0	841.29	846.75	854.30	854.23	0.65	1.55	1.54
85	0.1	0.9	831.50	830.62	794.83	790.05	0.11	4.41	4.99
90	0.2	0.8	795.10	791.14	785.39	789.79	0.50	1.22	0.67
	0	1	785.00	784.35	784.30	785.81	0.08	0.09	0.10
	0.6	0.4	815.70	811.52	819.78	808.00	0.51	0.50	0.94
	1	0	882.42	894.72	850.31	850.66	1.39	3.64	3.60
100	1	0	836.30	845.05	845.76	847.43	1.05	1.13	1.33
	0.1	0.9	799.60	795.81	785.87	783.67	0.47	1.72	1.99
120	1	0	850.08	859.06	831.36	834.21	1.06	2.20	1.87
130	1	0	815.00	835.72	819.19	820.14	2.54	0.51	0.63
140	1	0	845.05	853.54	801.98	859.35	1.01	5.10	1.69
180	1	0	656.85	653.61	690.28	669.69	0.49	5.09	1.95
200	1	0	886.43	901.09	885.30	880.52	1.65	0.13	0.67
220	1	0	606.93	611.58	616.10	595.96	0.77	1.51	1.81
280	1	0	545.25	531.78	534.51	523.85	2.47	1.97	3.92

Table 4.23: Evaluation of predictive models for the kinematic viscosity of Biodiesel

T [□]	Biodiesel fraction	Diesel fraction	Kinematic viscosity [mm^2/s]				Absolute error [%]		
			EXP	ANFIS	ANN	RBFNN	ANFIS	ANN	RBFNN
10	0.5	0.5	4.51	4.30	5.68	5.84	4.59	25.99	29.69
10	0.25	0.75	3.25	3.20	3.39	3.21	1.54	4.41	1.18
20	0.6	0.4	6.23	6.23	6.02	6.04	0.06	3.38	3.19
20	0.65	0.35	6.40	5.80	6.21	6.14	9.38	2.98	4.00
25	0.5	0.5	5.49	5.22	5.11	5.17	4.88	6.97	5.71
30	0.7	0.3	5.26	5.17	5.33	5.16	1.79	1.26	1.92
30	0.1	0.9	3.29	3.27	3.47	3.44	0.64	5.47	4.40
30	0.65	0.35	5.16	4.95	5.14	5.04	4.11	0.43	2.44
35	0.1	0.9	3.16	3.21	3.21	3.16	1.64	1.64	0.06
40	0.6	0.4	3.84	4.01	4.01	3.95	4.42	4.42	2.87
40	0.65	0.35	4.11	4.16	4.16	4.08	1.28	1.28	0.70
40	0.45	0.55	3.89	3.58	3.58	3.60	7.76	7.76	7.28
40	0.5	0.5	3.42	3.42	3.72	3.72	0.11	8.87	9.00
45	0.2	0.8	2.70	2.77	2.77	2.72	2.54	2.54	0.65
50	0.35	0.65	2.99	2.85	2.75	2.71	4.55	7.83	9.37
50	0.75	0.25	2.63	2.65	2.75	2.97	0.61	4.42	12.67
50	0.9	0.1	3.50	3.85	4.07	4.97	10.03	16.23	42.12
50	0.55	0.45	3.14	3.17	3.17	3.06	0.78	0.78	2.71
60	0.75	0.25	2.88	2.98	3.03	3.04	3.47	5.07	5.68
70	0.4	0.6	2.06	1.95	1.95	1.91	5.22	5.22	7.16
70	0.1	0.9	1.80	1.79	1.83	1.78	0.56	1.54	1.14
70	0.15	0.85	1.87	1.88	1.88	1.77	0.79	0.79	5.54
70	0.05	0.95	1.72	1.77	1.77	1.83	2.84	2.84	6.40
80	1	0	11.39	11.78	8.17	10.57	3.42	28.31	7.22
80	0.15	0.85	1.63	1.57	1.57	1.57	3.94	3.94	3.89
80	0.4	0.6	1.83	1.78	1.60	1.69	2.52	12.45	7.29
100	0.25	0.75	1.28	1.31	1.30	1.65	2.34	1.92	28.78
100	0.2	0.8	1.32	1.30	1.30	1.54	1.17	1.17	16.92
100	1	0	1.69	1.58	1.44	1.14	6.51	14.93	32.65
100	0.05	0.95	1.18	1.21	1.21	1.03	2.40	2.40	12.38
110	1	0	1.51	1.45	1.39	1.10	3.97	8.14	26.84
120	1	0	1.79	1.80	1.29	1.66	0.67	27.94	6.99
260	1	0	0.75	0.79	0.86	0.76	5.90	15.89	2.16
280	1	0	0.71	0.79	0.86	0.93	10.80	20.13	30.81

4.10 Evaluation of Predictive Current Models with Previous Study

4.10.1 Experimental Data

Kinematic viscosity data of different biodiesel blends samples at different temperatures were gathered from the literature. A total of 315 experimental data was obtained from scientific publication of Geacai et al., 2015, to estimate the kinematic viscosity of biodiesel blends. The development of the proposed approaches was performed as follows. In the first step, the experimental measurement data were separated into input data (independent variables, including temperature and volume fraction of biodiesel and output data (dependent variable in term of kinematic viscosity). Subsequently, different approaches (ANFIS and ANN) were proposed to describe the behavior of the kinematic viscosity, as a function of temperature and volume fraction of biodiesel. In this case, the database was randomly divided into three groups with 60% to training, 20% to testing and 20% to checking or validation. The temperature and volume fraction biodiesel were considered as input variables on ANFIS, ANN and RBFNN.

4.10.2 ANFIS Model

4.10.2.1 Method of Applications

The architecture of a two input with four rules ANFIS is shown as Figure 4.30. The ANFIS information and errors are shown in Table 4.24 that used for all biodiesel blends. Also the optimum method is hybrid. In this research, two methods, hybrid and back propagation tested for generation ANFIS that the results is presented in Tables 4.24 and 4.25 The results show the training error in the hybrid method is lower of back-propagation method. Therefore, the hybrid method has used for simulations.

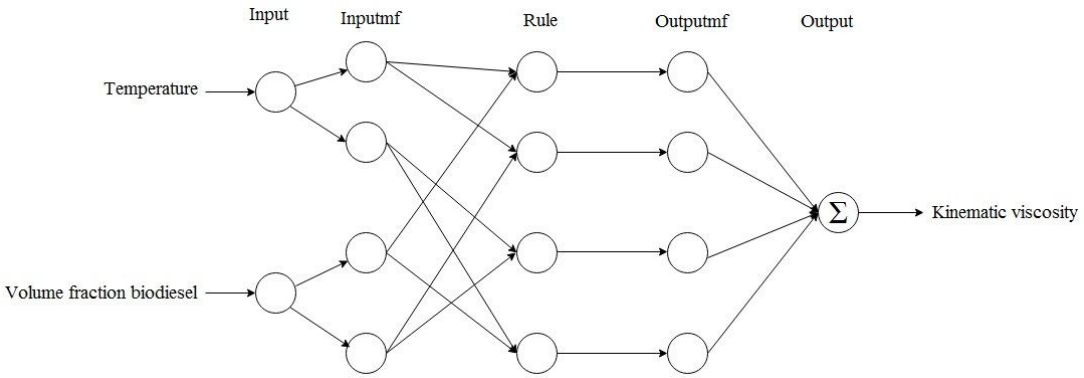

Figure 4.30: ANFIS architecture of two-input–single-output with twenty seven rules in biodiesel system

Table 4.24: The ANFIS information used in this study by the hybrid optimum method

	Biodiesel blend with Diesel	**Biodiesel blend with benzene**	**Biodiesel blend with toluene**
Epoch	1000	1000	1000
Training error	0.037	0.0155	0.0163
Tasting error	0.0469	0.0194	0.0154
Checking error	0.0408	0.0166	0.0171
Number of nodes	21	21	21
Number of linear parameters	4	4	4
Number of nonlinear parameters	8	8	8
Number of training data pairs:	43	43	43
Number of checking data pairs	20	20	20
Number of fuzzy rules	4	4	4

Table 4.25: The ANFIS information used in this study by back-propagation optimum method

	Biodiesel blend with Diesel	Biodiesel blend with benzene	Biodiesel blend with toluene
Epoch	1000	1000	1000
Training error	0.0384	0.0236	0.0246
Tasting error	0.0471	0.0227	0.0232
Checking error	0.0409	0.0229	0.0238
Number of nodes	21	21	21
Number of linear parameters	4	4	4
Number of nonlinear parameters	8	8	8
Number of training data pairs:	43	43	43
Number of checking data pairs	20	20	20
Number of fuzzy rules	4	4	4

4.10.2.2 ANFIS Model for Kinematic Viscosity of Biodiesel Blends

The influence of interactions of the two process input variables on the kinematic viscosity of biodiesel blends was graphically investigated using three dimensional surface plots as shown in Figure 4.31. Plots of the interaction between the temperature and volume fraction of biodiesel on kinematic viscosity of biodiesel blend with diesel fuel is described in Figure 4.31(a). The plots show that both variables significantly affect kinematic viscosity of biodiesel blend with diesel fuel. Also, the plots indicate that highest kinematic viscosity of biodiesel blend with diesel fuel can be achieved with increasing volume fraction of biodiesel (Figure 4.31(a)). The highest kinematic viscosity of biodiesel blend with diesel fuel can also be accomplished with decreasing the temperature (Figure 4.31(a)).

The three-dimensional surface plots of kinematic viscosity of biodiesel blend with benzene against temperature and volume fraction of biodiesel is depicted in (Figure 4.31 (b)). The plots suggest strong interaction between the variables with significant influence on the kinematic viscosity of biodiesel blend with benzene. From the Fig., increasing in volume fraction of biodiesel leads to increase the kinematic viscosity of biodiesel blend with benzene, while the lowest temperature leads to increase the kinematic viscosity of biodiesel blend with benzene as shown in Figure 4.31 (b).

The effect of the interaction of temperature and volume fraction of biodiesel on the kinematic viscosity of biodiesel blend with toluene is shown in Figure 4.31 (c). The Fig. suggests that both variables have significant influence on the kinematic viscosity of

biodiesel blend with toluene (Figure 4.31 (c)). Increasing the volume fraction of biodiesel, shows the kinematic viscosity of biodiesel blend with toluene increases. Conversely, increasing the temperature leads to decrease the kinematic viscosity of biodiesel blend with toluene as shown in Figure 4.31 (c).

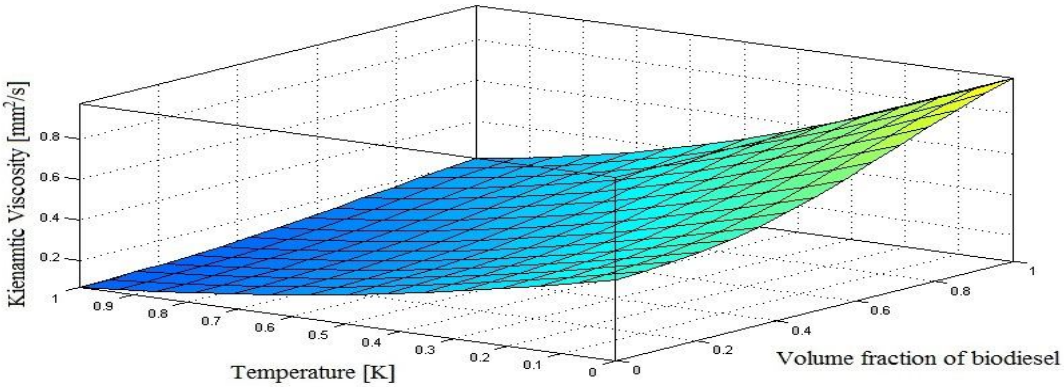

(a) Biodiesel blends with diesel

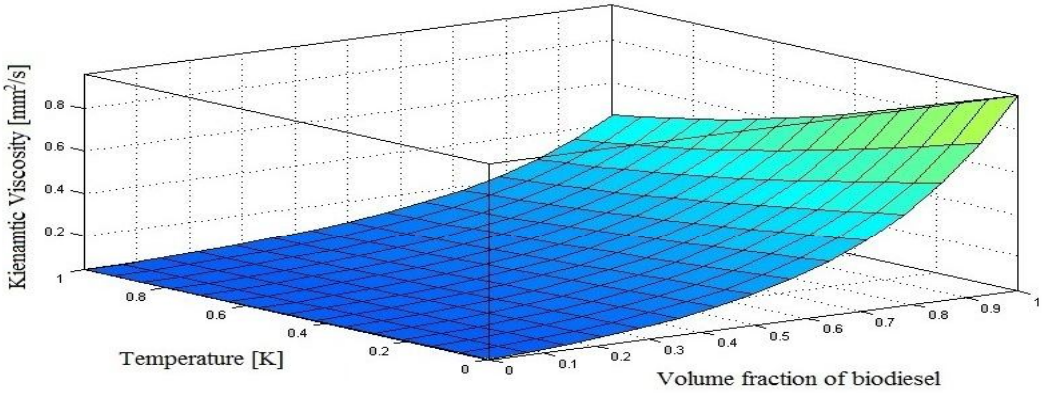

(b) Biodiesel blends with benzene

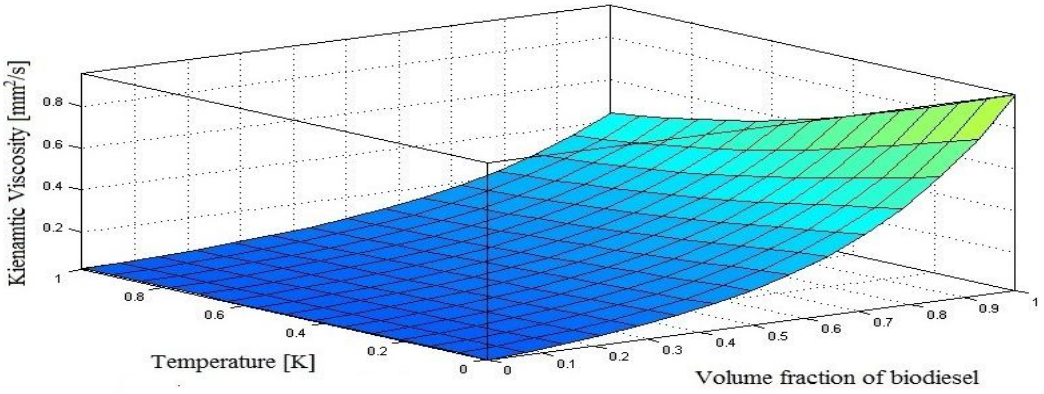

(c) Biodiesel blends with toluene

Figure 4.31: ANFIS prediction of maximal kinematic viscosity of biodiesel blends as function of temperature and volume fraction of biodiesel

4.10.3 ANN Models

In this model, 60% of the dataset were randomly selected as the training data, while the remaining 40% of the data was used for the performance test and validation of the ANN model. The back-propagation algorithm was chosen to calculate the weight values of the network. Choosing the optimum network architecture is one of the challenging steps in neural network modeling. A 2:2:1 ANN architecture with neurons in each layer has been used in this study as shown in Figure 4.32.

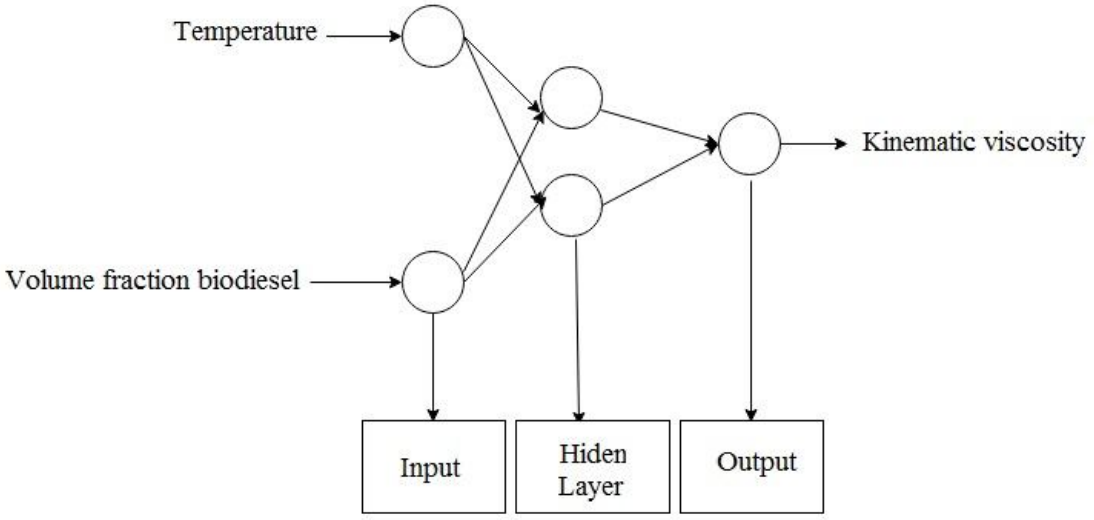

Figure 4.32: Neural network architecture

4.10.3.1 Modeling of Properties

A. Input Parameters

Figures 4.33, 4.34 and 4.35 show the straight lines for the training, validation, testing and performance of the network for biodiesel blends with diesel, benzene and toluene. For the trained network for estimating the kinematic viscosity, correlation coefficients (R) and the mean squared error (MSE) of biodiesel blends are shown in Table 4.26. The straight lines in Figures 4.33, 4.34 and 4.3.5 are the linear relationships obtained between the output (predicted) and the target (experimental) data of kinematic viscosity used in this present

study. The high coefficients of correlation obtained during the training, validation and testing of the kinematic viscosity network display very good relationship between the output and the experimental values of kinematic viscosity.

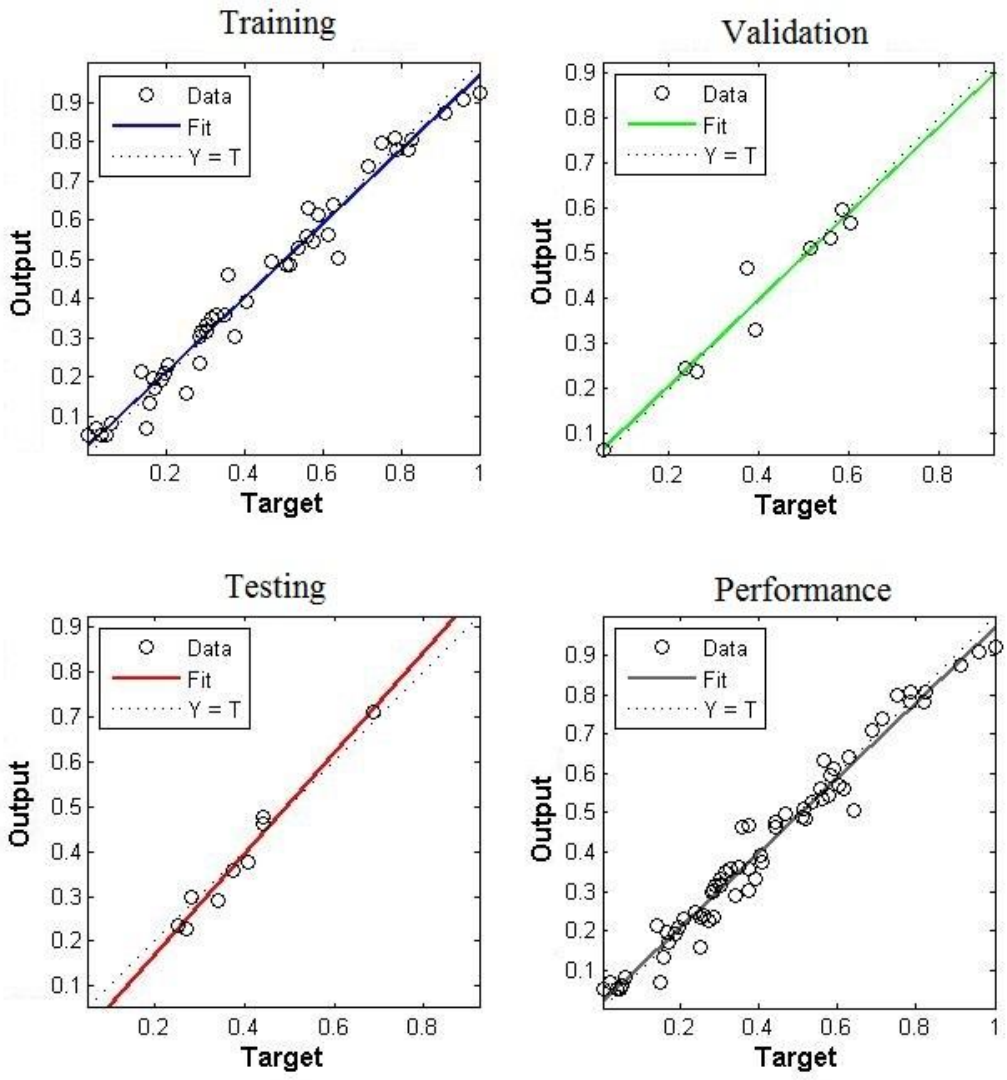

Figure 4.33: Regression plots for biodiesel blend with diesel fuel network

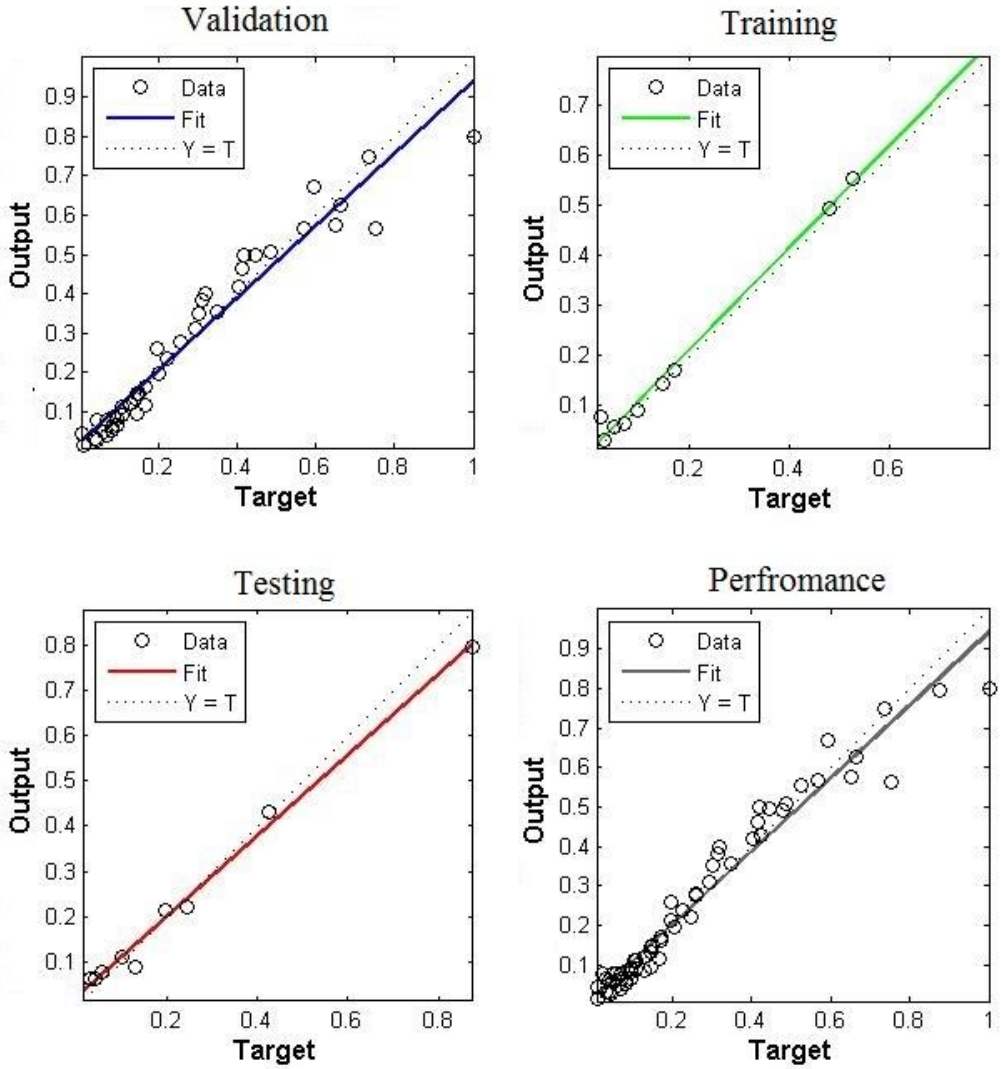

Figure 4.34: Regression plots for biodiesel blend with benzene network

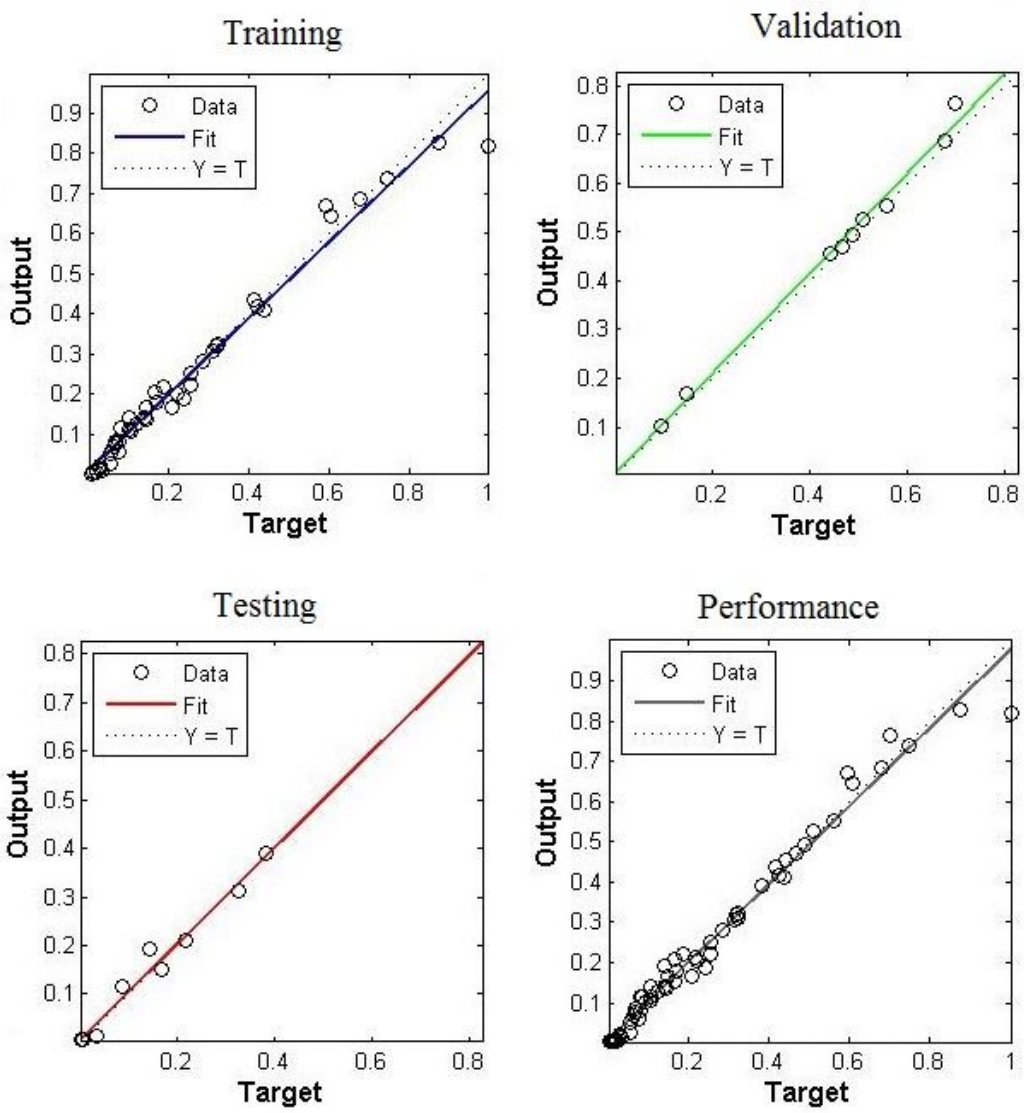

Figure 4.35: Regression plots for biodiesel blend with toluene network

Table 4.26: Performance of the network using Feed forward propagation for kinematic viscosity model

Biodiesel Blends	Training	Validation	Testing	Performance	MSE
Biodiesel blend with diesel fuel	0.985	0.973	0.984	0.984	0.00163
Biodiesel blend with benzene	0.973	0.995	0.995	0.979	0.000461
Biodiesel blend with toluene	0.989	0.996	0.986	0.990	0.000545

B. Output Parameters

The output parameters are the fuel properties (kinematic viscosity, density and dynamic viscosity) being predicted by the ANNs. Several ANNs with different hidden layers, number of neurons, transfer functions and training parameters are trained in order to determine the optimum hidden layer, number of neurons, transfer functions (pair) and training parameter's value, which would give the best prediction accuracy for each property.

4.10.3 Results of ANFIS and ANN Models

The predicted values obtained from the ANFIS and ANN model results were compared with experimental values as shown in Tables 4.27, 4.28 and 4.29 for biodiesel blend with diesel fuel, benzene and toluene, respectively. It is observed that the experimental results and the data obtained by ANFIS and ANN models are very close to each other.

It can be seen from these tables that as the volume fraction of biodiesel is increased, the kinematic viscosity of biodiesel blends is increased, whereas, kinematic viscosity of biodiesel blends decreased as the temperature increases. It was observed that the kinematic viscosity of biodiesel blends predicted using ANFIS approach is closed to kinematic viscosity of biodiesel blends obtained experimentally.

Table 4.27: Kinematic viscosity values of Biodiesel blend with diesel fuel using ANFIS and ANN

293.15K				298.15K			
V	ν [mm²/s]			V	ν [mm²/s]		
	experiment	ANFIS	ANN		experiment	ANFIS	ANN
0.55	6.098	6.083	6.089	0.5	5.488	5.492	5.408
0.5	5.971	5.971	5.841	0.25	5.072	5.056	5.166
0.2	5.438	5.440	5.441	0.75	6.114	6.107	6.158
0.6	6.234	6.258	6.335	0.65	5.848	5.862	5.921
0	5.331	5.346	5.046	0.3	4.522	4.496	5.138
0.7	6.576	6.662	6.640	0.05	4.878	4.859	5.019
0.3	5.56	5.540	5.466	0.1	4.925	4.916	5.145
0.15	5.412	5.427	5.417	0.85	6.429	6.439	6.629
0.85	7.168	7.181	7.013	0.15	4.968	5.034	5.190
303.15K				**313.15K**			
V	ν [mm²/s]			V	ν [mm²/s]		
	experiment	ANFIS	ANN		experiment	ANFIS	ANN
0.2	4.383	4.353	4.342	0.5	3.929	3.914	4.088
0	4.187	4.204	4.081	0.25	3.704	3.726	3.709
0.75	5.37	5.346	5.690	0.7	4.164	4.164	4.132
0.35	4.603	4.645	4.252	0.15	3.633	3.636	3.580
0.8	5.498	5.501	5.899	0.45	3.885	3.846	4.064
0.7	5.262	5.295	5.4708	0.05	3.567	3.603	3.311
0.25	4.447	4.441	4.291				
0.55	4.93	4.901	4.921				
323.15K							
V	ν [mm²/s]						
	experiment	ANFIS	ANN				
0.95	3.553	3.555	3.820				
0.15	2.86	2.814	3.205				
0.2	2.889	2.910	3.189				
0	2.792	2.822	2.986				
0.3	2.946	2.936	3.083				
0.55	3.144	3.166	3.368				
0.85	4.389	4.404	3.917				
0.1	2.832	2.826	3.157				
0.8	4.321	4.310	3.960				
0.65	4.11	4.101	3.804				

Table 4.28: Kinematic viscosity values of Biodiesel blend with benzene using ANFIS and ANN

293.15K				298.15K			
V	ν [mm^2/s]			V	ν [mm^2/s]		
	experiment	ANFIS	ANN		experiment	ANFIS	ANN
0.55	3.913	3.865	3.811	0.5	3.631	3.653	3.787
0.5	3.725	3.704	3.537	0.25	3.198	3.202	3.189
0.2	3.183	3.186	3.194	0.75	4.651	4.657	5.010
0.6	4.102	4.127	4.181	0.65	4.177	4.205	4.613
0	2.939	2.933	3.190	0.3	3.202	3.195	3.212
0.7	4.530	4.562	4.879	0.05	2.987	2.981	3.179
0.3	3.349	3.342	3.211	0.1	3.031	3.047	3.177
0.15	3.130	3.142	3.191	0.85	5.365	5.353	5.709
0.85	5.688	5.685	5.607	0.15	3.088	3.085	3.177
303.15K				**313.15K**			
V	ν [mm^2/s]			V	ν [mm^2/s]		
	experiment	ANFIS	ANN		experiment	ANFIS	ANN
0.2	3.070	3.096	3.080	0.5	3.398	3.402	3.307
0	2.881	2.868	3.139	0.25	3.075	3.108	2.959
0.75	4.447	4.445	4.439	0.7	3.923	3.930	4.041
0.35	3.272	3.289	3.160	0.15	2.981	2.999	2.940
0.8	4.655	4.668	4.870	0.45	3.334	3.330	3.197
0.7	4.246	4.216	4.114	0.05	2.896	2.876	2.980
0.25	3.136	3.140	3.084				
0.55	3.680	3.642	3.668				
323.15K							
V	ν [mm^2/s]						
	experiment	ANFIS	ANN				
0.95	4.672	4.726	4.842				
0.15	2.909	2.922	2.894				
0.2	2.950	2.948	2.916				
0	2.792	2.813	2.860				
0.3	3.061	3.063	2.980				
0.55	3.378	3.366	3.472				
0.85	4.547	4.426	4.570				
0.1	2.871	2.887	2.877				
0.8	4.269	4.146	4.398				
0.65	3.785	3.682	3.781				

Table 4.28: Kinematic viscosity values of Biodiesel blend with toluene using ANFIS and ANN

293.15K			
V	ν [mm²/s]		
	experiment	ANFIS	ANN
0.55	3.953766	3.96566	4.070596
0.5	3.80556	3.796158	3.892921
0.2	3.136175	3.105776	2.982933
0.6	4.171509	4.171264	4.233708
0	2.851001	2.841332	2.818873
0.7	4.611912	4.629688	4.60866
0.3	3.249261	3.232695	3.202694
0.15	3.04978	3.034215	2.901412
0.85	5.746284	5.808731	5.760374

298.15K			
V	ν [mm²/s]		
	experiment	ANFIS	ANN
0.5	3.675616	3.658365	3.746034
0.25	3.130556	3.113194	3.054225
0.75	4.697605	4.705427	4.671597
0.65	4.207331	4.201983	4.150262
0.3	3.136877	3.154626	3.210277
0.05	2.891038	2.917392	2.814958
0.1	2.937396	2.931292	2.825879
0.85	5.374716	5.383436	5.618728
0.15	3.002719	3.042517	2.856938

303.15K			
V	ν [mm²/s]		
	experiment	ANFIS	ANN
0.2	2.998505	2.994578	2.931575
0	2.846	2.838975	2.81104
0.75	4.437	4.451295	4.093624
0.35	3.224	3.204333	3.287606
0.8	4.685	4.695652	4.410325
0.7	4.230	4.246	3.883498
0.25	3.063	3.064	3.053055
0.55	3.699	3.682	3.557323

313.15K			
V	ν [mm²/s]		
	experiment	ANFIS	ANN
0.5	3.388336	3.338269	3.663898
0.25	3.002719	2.969135	2.94704
0.7	3.913026	3.901491	3.968254
0.15	2.914217	2.909679	2.8396
0.45	3.284381	3.296302	3.536915
0.05	2.839061	2.862972	2.819026

323.15K			
V	ν [mm²/s]		
	experiment	ANFIS	ANN
0.95	4.634	4.658	4.618
0.15	2.873	2.863	2.838
0.2	2.91	2.904	2.862
0	2.792	2.829	2.821
0.3	3.013	2.993	2.984
0.55	3.37	3.382	3.421
0.85	4.426	4.356	4.148
0.1	2.836	2.853	2.828
0.8	4.2389	4.252	4.017
0.65	3.745	3.734	3.696

4.10.4 RSM Models

The influence of temperature and volume fraction of biodiesel blends with diesel fuel, benzene and toluene on the kinematic viscosity was tested using RSM approach and comparing with the mathematical equation of Geacai et al., 2015, (appendix 1) . Each response was used to develop a mathematical model using RSM that correlates the kinematic viscosities to the independent reaction variables via polynomial equation as given below:

$$\nu(w,T) = p_{00} + p_{10}T + p_{01}w + p_{20}T^2 + p_{11}wT + p_{02}w^2 + p_{21}T^2w + p_{21}T^2w + p_{12}Tw^2 + p_{03}w^3 \quad (6.4)$$

where, $p_{00}, p_{10}, p_{01}, p_{20}, p_{11}, p_{02}, p_{12}, p_{21}, p_{12}$, and p_{03} are polynomial coefficients (Table 4.29).

Table 4.29 Polynomial equation coefficients for kinematic viscosity of biodiesel blends with diesel fuel

Polynomial equation coefficients	Value		
	Diesel fuel	Benzene	Toluene
p_{00}	46.09	4.613	-13.15
p_{10}	-0.1879	-0.01368	0.09767
p_{01}	133.9	48.08	135.6
p_{20}	0.000167	2.097E-06	-0.0001713
p_{11}	-0.8848	-0.3468	-0.9018
p_{02}	23.82	39.33	38.28
p_{21}	0.00146	0.0006412	0.001514
p_{12}	-0.0715	-0.1394	-0.1294
p_{03}	-0.3582	6.017	4.379

Figure 4.36, 4.37 and 4.38 present the accuracy of developed RSM predictive model for kinematic viscosity of biodiesel blends with diesel, benzene and toluene, respectively. It

can be seen that the most of the points fall along the diagonal line for the RSM compared to mathematical equations obtained by Geacai et al., 2015, prediction models. Consequently, it follows that prediction results using RSM are in very good agreement with the actual values of the kinematic viscosity of biodiesel. This observation can be confirmed with very high value of coefficient of determination.

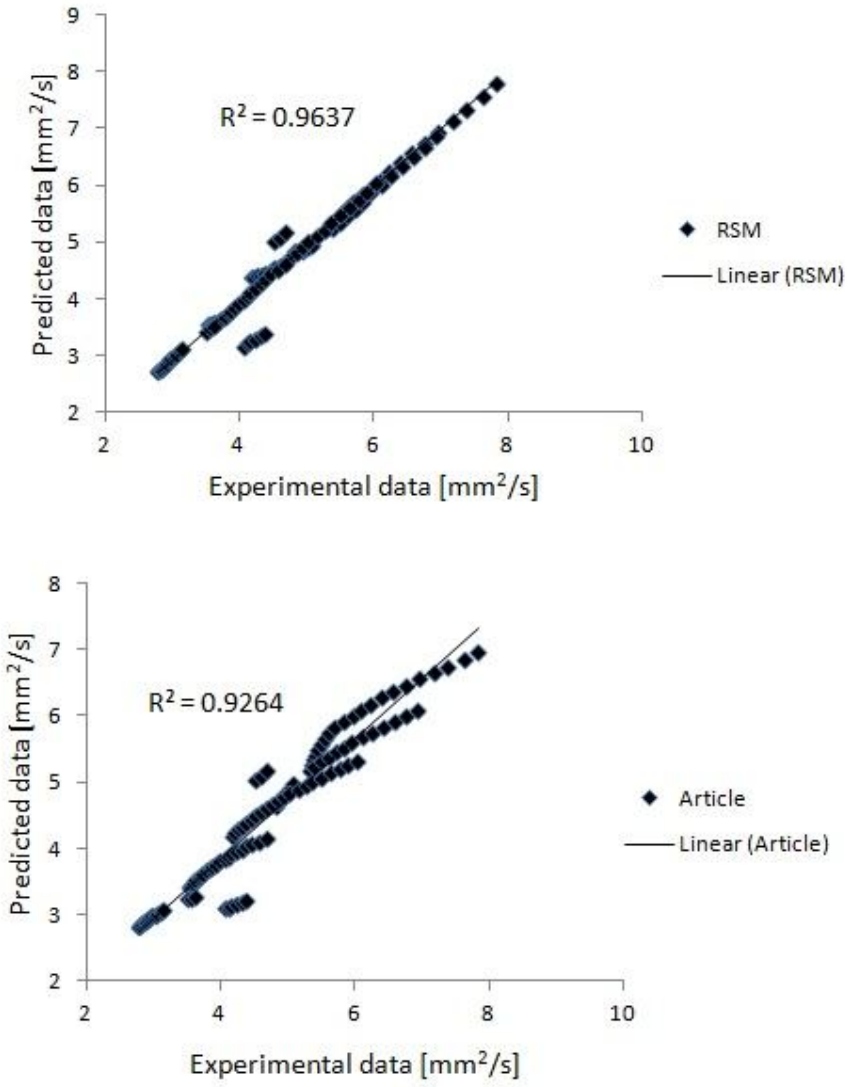

Figure 4.36: Fitting of the predicted ANFIS and experimental values for kinematic viscosity of biodiesel blends with diesel

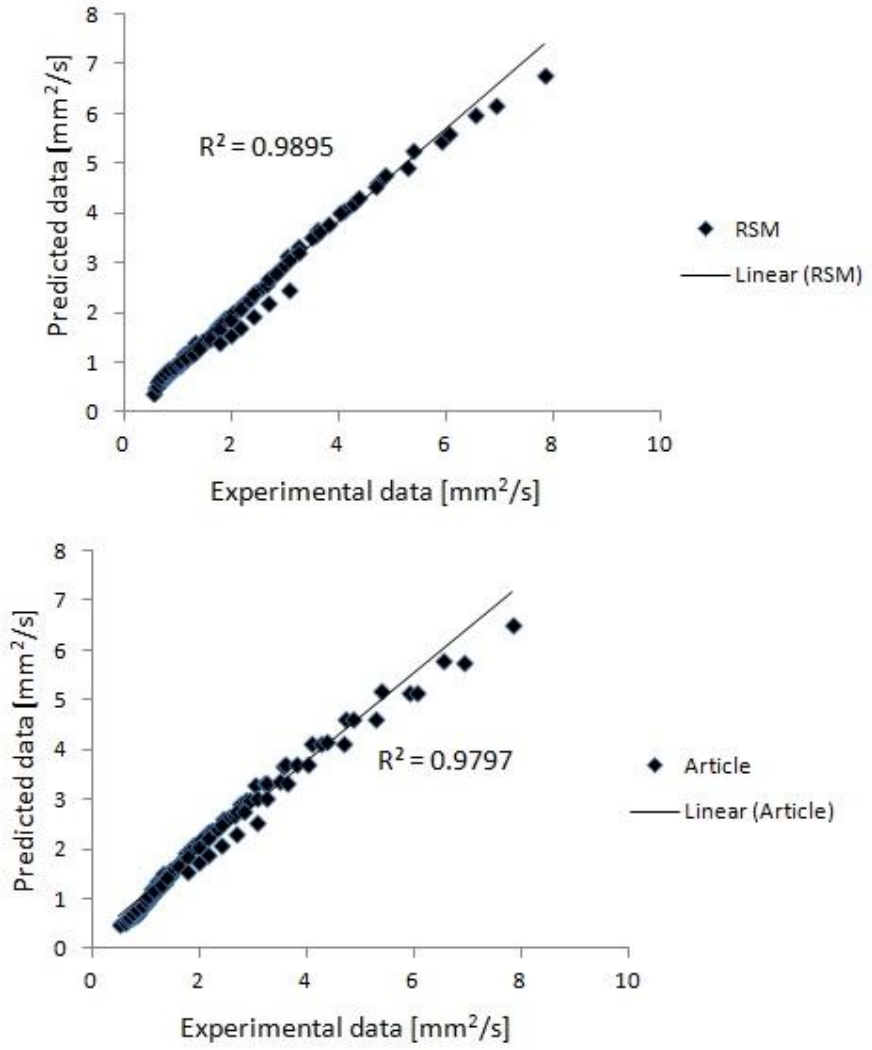

Figure 4.37: Fitting of the predicted ANFIS and experimental values for kinematic viscosity of biodiesel blends with benzene

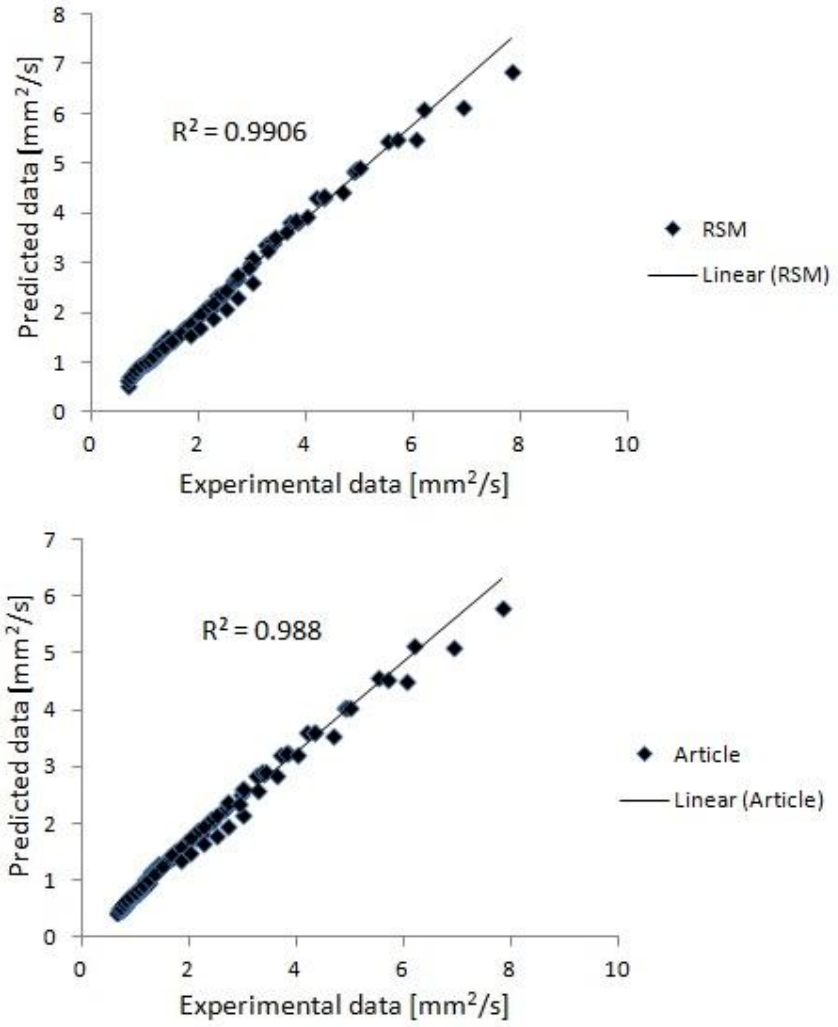

Figure 4.38: Fitting of the predicted ANFIS and experimental values for kinematic viscosity of biodiesel blends with toluene

CHAPTER 5
CONCLUSIONS

5.1 Conclusions

Viscosity and density are the most significant properties of biodiesel because of its major effect on the engine performance. For this reason reliable mathematical models that accurately describe the kinematic viscosity and density of biodiesel as a function of temperature and biodiesel fraction are of great interest for the development of combustion models as well as for the design of process equipment.

This work proves three empirical approaches, which are ANFIS, ANN and RBFNN to predict the density and kinematic viscosity of biodiesel blends at various temperatures and volume fraction of biodiesel, which is characterized by only three adjustable parameters.

Additionally, this study develops empirical equations using RSM methods to predict the density and kinematic viscosity of biodiesel blends at various temperatures and volume fraction of biodiesel as function of temperature and biodiesel fraction. Moreover, the results of empirical equations of kinematic viscosities for biodiesel blends with diesel fuel, benzene and toluene reported in the literature are compared well with the mathematical obtained using RSM approach of this work. The following conclusions can be drawn from the study:

- The densities and kinematic viscosity of diesel fuels are lower than biodiesels. Therefore, the density and kinematic viscosity of the blend increases with the increase of biodiesel concentration.
- The ANFIS, ANN, RBFNN and RSM methods used the temperatures and biodiesel fraction as inputs and the density and kinematic viscosity of biodiesel blends were output. Results indicate that the proposed ANFIS method is able to predict the most accurate biodiesel densities and kinematic viscosities with the overall R^2 of 0.95 compared with the other approaches.
- There is an excellent agreement between the experimental data and estimated values for the densities and kinematic viscosities.
- Overall, the ANFIS method presented the best accuracy with the highest *R-squared*.

- The statistical indices used in performance assessment of the developed models showed that the predictions of ANFIS, ANN and RBFNN models were more accurate than RSM model. Because of R-squared of these models is higher than RSM approach.
- According to the results, the mathematical equations obtained using RSM is better than mathematical equations obtained by Geacai et al., 2015 for calculating kinematic viscosity of blends. However, there is an excellent agreement between the experimental data and estimated values. Therefore, mathematical equations obtained using RSM can be used for predicting the viscosity of biodiesel blend without needing viscosity measurements.

REFERENCES

Aksoy, F., Baydir, Ş. A., & Bayrakçeken, H. (2009). The Viscosity at Different Temperatures of Soybean and Sunflower Biodiesels and Diesel Fuel Blends. *Energy Sources, Part A: Recovery, Utilization, and Environmental Effects*, *32*(2), 148-156.

Allen, C., Watts, K., Ackman, R., & Pegg, M. (1999). Predicting the viscosity of biodiesel fuels from their fatty acid ester composition. *Fuel*, *78*(11), 1319-1326.

Amin, A., Gadallah, A., El Morsi, A., El-Ibiari, N., & El-Diwani, G. (2016). Experimental and empirical study of diesel and castor biodiesel blending effect, on kinematic viscosity, density and calorific value. *Egyptian Journal of Petroleum*, *25*(4), 509-514.

Balabin, R. M., Lomakina, E. I., & Safieva, R. Z. (2011). Neural network (ANN) approach to biodiesel analysis: Analysis of biodiesel density, kinematic viscosity, methanol and water contents using near infrared (NIR) spectroscopy. *Fuel*, *90*(5), 2007-2015. doi:10.1016/j.fuel.2010.11.038

Barabás, I. (2013). Predicting the temperature dependent density of biodiesel–diesel–bioethanol blends. *Fuel*, *109*, 563-574.

Benjumea, P., Agudelo, J., & Agudelo, A. (2008). Basic properties of palm oil biodiesel–diesel blends. *Fuel*, *87*(10-11), 2069-2075.

Betiku, E., Adepoju, T. F., Omole, A. K., & Aluko, S. E. (2012). Statistical approach to the optimization of oil from beniseed (Sesamum indicum) oil seeds. *J Food Sci Eng*, *2*, 351-358

Billings, S. A., & Zheng, G. L. (1995). Radial basis function network configuration using genetic algorithms. *Neural Networks*, *8*(6), 877-890.

Castillo, O., & Melin, P. (2008). *Type-2 fuzzy logic: Theory and applications*. Berlin: Springer.

Cursaru, D. L., Tănăsescu, C., & Mărdărescu, V. (2011). Effect of biodiesel and alkyl ether on diesel engine emissions and performances. *Air Pollution XIX*. doi:10.2495/air110311

Cybenko, G. (1989). Approximation by superpositions of a sigmoidal function. *Mathematics of Control, Signals, and Systems* (MCSS), 2(4):303–314, 12 1989.

De Almeida, S. (2002). Performance of a diesel generator fuelled with palm oil. *Fuel*, *81*(16), 2097-2102.

Demirbas, A. (2008). Relationships derived from physical properties of vegetable oil and biodiesel fuels. *Fuel*, *87*(8-9), 1743-1748.

ElSolh, N. (2011). *The Manufacture of Biodiesel from the used vegetable oil* (Unpublished master's thesis). Cairo University, Egypt.

Esteban, B., Riba, J., Baquero, G., Rius, A., & Puig, R. (2012). Temperature dependence of density and viscosity of vegetable oils. *Biomass and Bioenergy*, *42*, 164-171.

Freitas, S. V., Pratas, M. J., Ceriani, R., Lima, A. S., & Coutinho, J. A. (2011). Evaluation of Predictive Models for the Viscosity of Biodiesel. *Energy & Fuels*, *25*(1), 352-358. doi:10.1021/ef101299d

Freitas, S. V., Pratas, M. J., Ceriani, R., Lima, A. S., & Coutinho, J. A. (2011). Evaluation of Predictive Models for the Viscosity of Biodiesel. *Energy & Fuels*, *25*(1), 352-358.

Freitas, S. V., Segovia, J. J., Carmen Martín, M., Zambrano, J., Oliveira, M. B., Lima, Á. S., & Coutinho, J. A. (2014). Measurement and prediction of high-pressure viscosities of biodiesel fuels. *Fuel*, *122*, 223-228.

Geacai, S., Iulian, O., & Nita, I. (2015). Measurement, correlation and prediction of biodiesel blends viscosity. *Fuel*, *143*, 268-274.

Gouw, T. H., & Vlugter, J. C. (1964). Physical properties of fatty acid methyl esters. I. density and molar volume. *Journal of the American Oil Chemists' Society*, *41*(2), 142-145.

Gülüm, M., & Bilgin, A. (2016). Two-term power models for estimating kinematic viscosities of different biodiesel-diesel fuel blends. *Fuel Processing Technology*, *149*, 121-130.

Haykin, S. (1995). *Neural networks: A comprehensive foundation*. New York, NY [u.a.: Macmillan.

Haykin, S. S. (2009). *Neural networks and learning machines*. New York: Prentice Hall/Pearson.

Ivaniš, G. R., Radović, I. R., Veljković, V. B., & Kijevčanin, M. L. (2016). Thermodynamic properties of biodiesel and petro-diesel blends at high pressures and temperatures. Experimental and modeling. *Fuel*, *184*, 277-288. doi:10.1016/j.fuel.2016.07.023

Jang, J. -S., Sun, C.-T, & Mizutani, E. (1997). *Neuro-fuzzy and soft computing: A computational approach to learning and machine intelligence*. Upper Saddle River, NJ: Prentice Hall.

Jang, J., & Sun, C. (1993). Functional equivalence between radial basis function networks and fuzzy inference systems. *IEEE Transactions on Neural Networks, 4*(1), 156-159.

Kanaveli, I., Atzemi, M., & Lois, E. (2017). Predicting the viscosity of diesel/biodiesel blends. *Fuel, 199*, 248-263.

Knothe, G., & Steidley, K. R. (2007). Kinematic viscosity of biodiesel components (fatty acid alkyl esters) and related compounds at low temperatures. *Fuel, 86*(16), 2560-2567.

Krisnangkura, K., Yimsuwan, T., & Pairintra, R. (2006). An empirical approach in predicting biodiesel viscosity at various temperatures. *Fuel, 85*(1), 107-113.

Liu, D., Zhang, H., Alippi, C., Polycarpou, M., & He, H. (2011). *Advances in Neural Networks - ISNN 2011: 8th International Symposium on Neural Networks, ISNN 2011, Guilin, China, May 29-June 1, 2011, Proceedings, Part II*. Berlin, Heidelberg: Springer Berlin Heidelberg.

Ma, F., & A Hanna, M. (1999). Biodiesel production: a review. *Bioresource Technology, 70*(1), 1-15.

Ma, F., Clements, L., & Hanna, M. A. (1999). The effect of mixing on transesterification of beef tallow. *Bioresource Technology, 69*(3), 289-293.

Machado, M., Zuvanov, V., Rojas, E., Zuniga, A., & Costa, B. (2012). Thermo physical Properties of Biodiesel Obtained From Vegetable Oils: Corn, Soy, Canola And Sunflower. *ENCICLOPÉDIA BIOSFERA,, 8*(14), 917.

Manohar, B., & Divakar, S. (2005). An artificial neural network analysis of porcine pancreas lipase catalysed esterification of anthranilic acid with methanol. *Process Biochemistry, 40*(10), 3372-3376.

Mejía, J., Salgado, N., & Orrego, C. (2013). Effect of blends of Diesel and Palm-Castor biodiesels on viscosity, cloud point and flash point. *Industrial Crops and Products, 43*, 791-797.

Meng, X., Jia, M., & Wang, T. (2014). Neural network prediction of biodiesel kinematic viscosity at 313K. *Fuel, 121*, 133-140.

Misra, R., & Murthy, M. (2010). Straight vegetable oils usage in a compression ignition engine—A review. *Renewable and Sustainable Energy Reviews, 14*(9), 3005-3013.

Moradi, G., Mohadesi, M., Karami, B., & Moradi, R. (2015). Using Artificial Neural Network for Estimation of Density and Viscosities of Biodiesel–Diesel Blends. *Journal of Chemical and Petroleum Engineering, 49*(2), 153-165.

Nasiri, H. G., Mosavian, M. T., Kadkhodaee, R., & Sargolzae, J. (2013). Modeling of Oil-Water Emulsion Separation in Ultrasound Standing Wavefield by Neural Network. *Journal of Dispersion Science and Technology, 34*(4), 490-495.

Nelles, O. (2001). *Nonlinear system identification: From classical approaches to neural networks and fuzzy models*. Berlin: Springer.

Piloto-Rodríguez, R., Sánchez-Borroto, Y., Lapuerta, M., Goyos-Pérez, L., & Verhelst, S. (2013). Prediction of the cetane number of biodiesel using artificial neural networks and multiple linear regression. *Energy Conversion and Management, 65*, 255-261.

Pinto, A., Guarieiro, L., Rezende, M., Lopes, W., Pereira, P., & Andrade, J. (2005). Biodiesel: an overview. *Journal of the Brazilian Chemical Society, 16*, 1313-1330. Retrieved from

Pratas, M. J., Freitas, S. V., Oliveira, M. B., Monteiro, S. C., Lima, A. S., & Coutinho, J. A. (2011). Biodiesel Density: Experimental Measurements and Prediction Models. *Energy & Fuels, 25*(5), 2333-2340.

Ramírez-Verduzco, L. F., García-Flores, B. E., Rodríguez-Rodríguez, J. E., & Del Rayo Jaramillo-Jacob, A. (2011). Prediction of the density and viscosity in biodiesel blends at various temperatures. *Fuel, 90*(5), 1751-1761.

Saldana, D. A., Starck, L., Mougin, P., Rousseau, B., Ferrando, N., & Creton, B. (2012). Prediction of Density and Viscosity of Biofuel Compounds Using Machine Learning Methods. *Energy & Fuels, 26*(4), 2416-2426.

Sarimveis, H., Alexandridis, A., Tsekouras, G., & Bafas, G. (2002). A Fast and Efficient Algorithm for Training Radial Basis Function Neural Networks Based on a Fuzzy Partition of the Input Space. *Industrial & Engineering Chemistry Research, 41*(4), 751-759.

Srinivasa, P. (2004). *Acoustic emission based tool wear monitoring using some improved neural network methodologies* (Unpublished doctoral dissertation). University of Mysore, India.

Srinivasa, P., Nagabhushan, T. N., & Ramakrishna Rao, P. K. (2003). Radial basis function neural networks for tool wear monitoring. *International Journal of COMADEM*, *5*(3), 21-30.

Tate, R., Watts, K., Allen, C., & Wilkie, K. (2006). The densities of three biodiesel fuels at temperatures up to 300°C. *Fuel*, *85*(7-8), 1004-1009.

Tate, R., Watts, K., Allen, C., & Wilkie, K. (2006). The viscosities of three biodiesel fuels at temperatures up to 300°C. *Fuel*, *85*(7-8), 1010-1015.

Taylor, J. G. (1996). *Neural networks and their applications*.

Tesfa, B., Mishra, R., Gu, F., & Powles, N. (2010). Prediction models for density and viscosity of biodiesel and their effects on fuel supply system in CI engines. *Renewable Energy*, *35*(12), 2752-2760.

Tsukamoto, Y., Gupta, M. M., Ragade, R. K., & Yager, R. R. (1979). An approach to fuzzy reasoning method," in *Advances in Fuzzy Set Theory and Application. North-Holland, Amsterdam*. pp. 137–149.

Vicente, G., Martí nez, M., & Aracil, J. (2004). Integrated biodiesel production: a comparison of different homogeneous catalysts systems. *Bioresource Technology*, *92*(3), 297-305.

Yuan, W., Hansen, A. C., Zhang, Q., & Tan, Z. (2005). Temperature-dependent kinematic viscosity of selected biodiesel fuels and blends with diesel fuel. *Journal of the American Oil Chemists' Society*, *82*(3), 195-199.

Zha, X. F., & Howlett, R. J. (2006). *Integrated intelligent systems for engineering design*.